

Creatine Chemical Exchange Saturation Transfer Imaging and
Arterial Spin Labeling in the Study of Peripheral Arterial
Disease

A

Thesis

Presented to

the faculty of the School of Engineering and Applied Science
University of Virginia

in partial fulfillment
of the requirements for the degree

Doctor of Philosophy

by

Helen Sporkin

May 2024

APPROVAL SHEET

This
Thesis
is submitted in partial fulfillment of the requirements
for the degree of
Doctor of Philosophy

Author: Helen Sporkin

This Thesis has been read and approved by the examining committee:

Advisor: Craig H. Meyer

Advisor:

Committee Member: Frederick H. Epstein

Committee Member: Christopher M. Kramer

Committee Member: G. Wilson Miller

Committee Member: Jason D. Allen

Committee Member:

Committee Member:

Accepted for the School of Engineering and Applied Science:



Jennifer L. West, School of Engineering and Applied Science

May 2024

Acknowledgements

I would like to dedicate this thesis to my daughter, Leora, whose laugh and smile inspire me daily. I would like to thank my husband, Erik, who not only became the most impressive father and husband, additionally cheered me on from many low points in my research from which I thought this project would not recover. His many hours of brainstorming, practice talks, and time spent in the MRI as a research subject are without doubt proof of his deep love for me and radiologic research. I would like to express my deepest gratitude to my mother-in-law, Cheryl, who watched Leora with as much love and care as possible and allowed me to complete this thesis without worry. I would also like to thank my mother for her encouragement and support throughout my life. Without her belief in me I would never have followed my heart and studied science. I am deeply saddened that my father and grandmother did not live to see me graduate, and I can only hope my accomplishments continue to make their spirits proud.

I am so grateful for a supportive and knowledgeable lab environment created by my advisor, Dr. Craig Meyer. When I started in the lab as the lone graduate student with very little MRI experience, Dr. Meyer and our post docs, Dr. Steven Allen and Dr. Xue Feng, took me in and taught me everything I needed to know and more. To my lab mates through the years, Katya Gilbo, Quan Dou, Zhixing Wang, Shen Chen, and Kang Yan, thank you for the laughs and support through the years. I look forward to seeing all the great work you do in your promising futures.

For her endless support and clinical knowledge, I would like to thank Jennifer Kay BSN. To my cardiac imaging fellows Roshin Mathew, Christopher Schumann, Toral Patel, and Yakub Betz, thank you for your help with assisting the subjects, wrangling the data, writing, and all the laughs as the scanner buzzed on. I would like to thank Dr. Jason Allen and his lab, particularly Dr. Joaquin Ortiz de Zevallo, for bringing me on to their exciting project. Many thanks to Dr. Wilson Miller, who taught me the ropes of running the scanners and MRI physics and emergency troubleshooting countless time sensitive errors. Thank

you, Dr. Fredrick Epstein, for chairing my committee and being a wonderful teacher. Great thanks to Dr. Christopher Kramer, for creating this project and being a supportive advisor and inspiring clinician scientist.

I acknowledge and thank Dr. Hari Hariharan and Dr. Neil Wilson from the University of Pennsylvania for MRI pulse sequences and processing software. This project was supported by the National Institute of Health grants R01 HL075792, T32 HL007284, T32 EB003841, and the University of Virginia's 3 Cavalier's grant. The CEST software was made available through P41 EB015893.

Table of Contents

Abstract

Chapter 1: Significance

Chapter 2: Background

- 2.1 Magnetic resonance
- 2.2 Relaxation
- 2.3 Off-resonance
- 2.4 Phosphorous-31 magnetic resonance spectroscopy
- 2.5 Chemical exchange saturation transfer imaging
- 2.6 Magnetization Transfer
- 2.7 Phosphocreatine Metabolism
- 2.8 Arterial spin labeling
- 2.9 Ergometry
- 2.10 Peripheral arterial disease
- 2.11 Revascularization
- 2.12 Nitrate

Chapter 3: CrCEST method can distinguish creatine kinetics in PAD patients compared to age matched controls

- 3.1 Rationale
- 3.2 Methods
- 3.3 Statistical Analysis
- 3.4 Results
- 3.5 Discussion
- 3.6 Limitations

Chapter 4: MRI methods to study the relationship of changes in perfusion and energetics with revascularization in PAD

- 4.1 Rationale
- 4.2 Methods
- 4.3 Statistical Analysis
- 4.4 Results
- 4.5 Discussion
- 4.6 Limitations

Chapter 5: ***Future plans- Creating a combined CrCEST and ASL imaging protocol***

- 5.1 Introduction
- 5.2 Future Work
- 5.3 Conclusions

Appendix

References

Figures and Tables

Figure 1: The precession of a magnetic moment around the effective magnetic field in the rotating reference frame.^[51]

Figure 2: From Isbell 2006, a non-spatial ^{31}P spectrum showing relative quantities of phosphorous species in calf skeletal muscle.^[6]

Figure 3: Spectral frequencies of bound and free proton pools.

Figure 4: The nuclear Overhauser effect leading to magnetization transfer and its effect on magnetization.

Figure 5: The effect of magnetization transfer imaging preparation pulses on magnetization.

Figure 6: Phosphocreatine metabolism.

Figure 7: The CEST effect during creatine rephosphorylation and its effect on magnetization

Figure 8: An example of a z-spectrum of creatine rich tissue.^[68]

Figure 9: First stage prototype ergometer

Figure 10: Schematic of the upgraded ergometer, the Trispect from Ergospect

Figure 11: Calf muscle maps, chemical exchange saturation transfer asymmetry maps, and regions of interest with decay curves

Figure 12: Example chemical exchange saturation transfer (CEST) images and corresponding CEST asymmetry ($\text{CEST}_{\text{asym}}$) decay curves from a normal control (top) and a patient with peripheral artery disease (PAD).

Figure 13: Bland-Altman plot comparing test-retest values in a total of 10 subjects

Figure 14: Bland-Altman plot comparing PCr recovery time constant by ^{31}P MRS and $\text{CEST}_{\text{asym}}$ decay constant for 13 patients with peripheral artery disease and 11 normal controls.

Figure 15: Pearson correlation plot of chemical exchange saturation transfer (CEST) decay constant versus phosphocreatine recovery time constant. $P=0.66$, $r=0.09$.

Figure 16: Total patient recruitment arm structure under Aim 2.

Figure 17: Collapsed recruitment arm structure under Aim 2.

Figure 18: CrCEST and ASL results from a 39-year-old patient with intermittent claudication due to iliac artery compression

Figure 19: Non-intervention subject health outcomes

Figure 20: Q2TIPS pulse sequence diagram

Figure 21: An example of locations of the in-plane presaturation slab, imaging slices, periodic saturation slice, and inversion slab from the PICORE tagging scheme in the leg.

Figure 22: pCASL tagging scheme.

Figure 23: Simplified timing diagram of our CEST pulse sequence

Figure 24: Simplified timing diagram of the pCASL sequence

Figure 25: Simplified timing diagram of the PASL sequence

Figure 26: Simplified timing diagram of our CEST and ASL pulse sequence

Table 1: Demographics of the Study Population

Table 2: CEST_{asym} Results

Table 3. Data From PAD and Controls Undergoing Both CEST and ³¹P MRS Post Exercise

Table 4: ABI, CEST, ASL, and 6-min walk score changes post-revascularization

Table 5: ABI, CEST, ASL, and 6-min walk score correlation results post-revascularization

Table 6: Beet juice subject characteristics

Table 7: CEST_{asym} decay results for the beetroot juice supplementation group

Table 8: ASL flow results for the beetroot juice supplementation group

Abstract

The major goal of my research was to develop a creatine chemical exchange saturation transfer (CrCEST) and Arterial Spin Labeling (ASL) imaging protocol for the study of peripheral arterial disease (PAD). Phosphocreatine metabolism is vital in highly oxidative tissues, such as the skeletal muscle of the limbs. Atherosclerotic diseases like PAD compromise downstream tissue perfusion, causing ischemia. ³¹Phosphorus MR spectroscopy (³¹P MRS) has demonstrated a delayed phosphocreatine (PCr) recovery time constant after exercise in PAD patients compared to healthy subjects, but this method suffers from low SNR, does not produce an image, and requires multi-nuclear scanner hardware. CrCEST is a developing MRI method capable of quantitatively imaging creatine concentration that does not require multinuclear hardware and can be reliably performed at 3T field strength. This is a particularly unique imaging method for PAD that can provide quantitative functional and spatial information at a muscle group level. This can then be matched to muscle group perfusion quantification using techniques such as arterial spin labeling (ASL). We hypothesized that creatine kinetics provided by CrCEST can both distinguish between PAD patients and healthy controls and differentiate between responders and non-responders to revascularization therapy. The goal of this project was to determine whether a CrCEST time series imaging protocol is capable of studying metabolic dysfunction in the skeletal muscle of patients with PAD and monitor disease progression and functional outcomes. We studied the relationship between metabolism and perfusion using CrCEST and arterial spin labeling MRI (ASL) in patients undergoing revascularization. This combined imaging protocol assessed changes post-procedure in patients undergoing both endovascular angioplasty and surgical bypass to treat intermittent claudication and critical limb ischemia, and correlate imaging findings with functional changes in six-minute walk score metrics. Additionally, we developed a combined ASL and CEST imaging sequence capable of assessing metabolism and perfusion in a single post-exercise session. This allows faster imaging times, and reduced pain for patients with difficulty exercising.

We hypothesized that ischemia in PAD leads to altered creatine concentration decay post-exercise in patients compared to age-matched controls. The effects of PAD on creatine metabolism are not fully understood, but prior studies with ^{31}P MRS show an observable and repeatable difference in metabolism for PAD patients.^[6] We also tested the ability of CrCEST to do so on a muscle group basis. Subjects performed plantarflexion ergometry to exhaustion or claudication using a calf ergometer that is capable of uniformly activating the calf muscles.

We hypothesized that the shapes of creatine concentration decays post-exercise will change in response to treatment and provide information that will correlate with disease progression and functional outcomes. We scanned patients before and after surgical and endovascular revascularization, patients not receiving treatment, and receiving inorganic nitrate supplementation. Each imaging session included an exercise CrCEST protocol, followed by exercise-induced hyperemia ASL in order to compare the metabolism information from CrCEST to perfusion. This novel methodology provides a map of vascular and mitochondrial kinetics in the skeletal muscle that can be analyzed down to the muscle group level. The imaging protocol developed for the revascularization assessment involves two exercise periods to establish sufficient perfusion and metabolic endogenous contrast within the tissue. This extends total scanner use time and is painful for patients. We developed a single imaging sequence that can measure both CEST and ASL signal within the period of post-exercise hyperemia and increased metabolic energetics seen after plantarflexion.

Chapter 1: Significance

Perfusion of oxygenated blood is necessary for the survival of all tissue within the human body.

Atherosclerotic disease is the largest cause of death globally; most commonly leading to mortality through ischemic stroke and heart disease.^[1] Peripheral arterial disease (PAD) is another major atherosclerotic disease affecting over 200 million worldwide, and is characterized by atherosclerotic

lesions in the arteries supplying one or more limbs, leading to decreased perfusion in the tissue.^[1] PAD is generally defined as a patient having an ankle brachial index (ABI) of <0.9. PAD leads to a major morbidity burden with over 5% of the general population over 40 being affected in the US.^[2,3] Symptoms can severely limit mobility, and involve pain, weakness, and claudication, usually affecting the lower limbs. Within 5 years of diagnosis, 1-2% of patients will progress to critical limb ischemia (CLI) and will require a revascularization procedure or amputation, further limiting their mobility and quality of life.^[4] Within 1 year of progression to CLI, 25% of patients will undergo an amputation, and 25% will experience CV mortality.^[2,30] There is an unmet clinical need to understand the mechanisms and causes of progression of PAD in the lower limbs to improve treatment outcomes in patients.^[1] The standard diagnostic test for identifying PAD is the ABI with doppler ultrasound. This is highly specific at the <0.9 level but decreasing ABI does not correlate well with worsening function or outcomes.^[8,31] Incompressible vessels as a result of vessel calcification also cause erroneously high ABI readings of >1.3. While ABI is useful in the screening of PAD, 6-minute walk scores remain the best endpoint in assessing function in PAD patients^[8,31], but this can be affected by disease in either limb. After revascularization procedures, the ABI frequently increases in patients with no benefit in functional improvement for the patient or the limb.^[4] ABI is a measure of bulk arterial flow and not indicative of tissue perfusion as has been shown using MR arterial spin labeling (ASL).^[6,7,8] A major challenge for the development of new therapies is the lack of quantitative measures for measuring tissue physiology such as energetics and perfusion. Large vessel inflow as measured by ABI and angiography does not reflect the tissue effects of therapies. CrCEST offers such promise as an attractive target for assessing benefits of revascularization, other novel therapies, and clinical outcomes in PAD.

One technique to assess calf muscle physiology, specifically energetics, is phosphorus-31 (³¹P) magnetic resonance spectroscopy (MRS).^[6] Phosphocreatine is used in the tissue as a secondary energy source to rephosphorylate adenosine diphosphate (ADP) after use without the need for aerobic

respiration. After exertion, the phosphate group of phosphocreatine is expended and joins the free phosphate pool within the tissue until oxidative phosphorylation can occur in the mitochondria. Prolonged phosphocreatine recovery kinetics have been shown to be indicative of tissue ischemia in PAD.^[6] ³¹P MRS has been available since the 1980s for evaluation of PAD, but suffers from low signal-to-noise ratio due to the low concentration of phosphocreatine and small gyro- magnetic ratio leading to a low NMR sensitivity to ³¹P.^[6] Specialized imaging hardware is necessary for detecting nuclei other than hydrogen and is frequently unavailable in clinical settings. Additionally, MRS typically results in frequency spectra rather than traditional images and has limited spatial resolution.^[5] CrCEST is an imaging technique that does not require multispectral hardware and thus could theoretically be applied on any high field clinical scanner with the appropriate pulse sequence and thus has far broader clinical potential than ³¹P MRS. In addition, the ability to localize abnormal energetics to individual muscle groups could allow the development of vessel and thus muscle-specific revascularization therapies. Our group has developed novel non-contrast methods of measuring tissue perfusion in PAD subjects using arterial spin labeling (ASL) MRI after exercise or with thigh cuff occlusion/hyperemia.^[11,15] Similarly to CrCEST, perfusion can be measured by ASL on a per muscle group basis. Combining these non-contrast measures of perfusion and energetics could offer significant potential for understanding the physiologic effects of revascularization and novel medical therapies on specific muscle groups in the calf. Perfusion as measured with single photon emission tomographic techniques has been shown to be an important marker of prognosis, predicting amputation-free survival in PAD.^[13] Future studies will help determine whether perfusion, energetics, or the combination are the best predictors of PAD outcome. Our study used CrCEST and ASL to monitor improvements as a result of interventions. This was the first study comparing metabolic and perfusion imaging to functional outcomes like the 6-min walk score and limb outcomes. Oral inorganic nitrate supplementation through beet juice has been shown to increase plasma nitric oxide levels and decreases claudication symptoms in PAD patients shown through

significant increases in exercise tolerance.^[43] Our imaging protocol demonstrates whether there are significant changes in metabolism or perfusion accompanying any improvements in 6-min walk score as a result of this supplementation.

Chapter 2: Background

2.1. Magnetic Resonance (MR)

Nuclear magnetic resonance (NMR) spectroscopy has been used to distinguish molecular composition of substances since 1938.^[56] Proton spins within the molecules of a substance in a static magnetic field precess at a specific frequency that allows for their identification and quantification.^[56] ^[50] This method can also be applied in two dimensions to form an image with voxels representing a spatial map of quantitative measures of the specie of interest. Magnetic resonance imaging (MRI) uses this method to create images for use in medical imaging. The formation of the signal in MRI relies on the alignment of rotating protons in the imaged object to a static external magnetic field (B_0) provided by the MRI scanner. These protons will precess about the main B_0 field in the longitudinal direction with angular frequency ω_0 , known as the Larmor frequency

$$\omega_0 = \gamma B_0 \quad 2 - 1$$

[51][52]

where γ is the gyromagnetic ratio of the protons being imaged.^{[51][52]} The longitudinal magnetization of the proton spins within the object of interest when placed in the B_0 field is expressed as

$$M_0 = \frac{\rho_0 \gamma^2 \hbar^2}{4kT} B_0, \quad \hbar = \frac{h}{2\pi} \quad 2 - 2$$

[51][52]

where ρ_0 is the proton density of the object, h is Plank's constant, k is Boltzmann's constant, and T is temperature. From this, the magnetization of the protons in the object of interest is proportional to the factors shown in equation 2-3.

$$M \propto \frac{\gamma^2 B_0 \rho_0}{T} \quad 2 - 3$$

[51]

Assuming that the temperature is not a modifiable constant (as with a human subject), the gyromagnetic ratio and proton density remain as the variable factors. Water is the most abundant molecule in the human body, making up around 70% of an adult.^[58] The proton of ¹H within the water molecule has a gyromagnetic ratio of 42.576 MHz/T, the highest of any molecule present in the human body.^{[51][52]} The ¹H protons in water form the signal for the majority of MRI methods due to this resulting high magnetization. The strength of the B_0 field is dependent on the scanner being used, with 1.5 and 3T scanners being most common for human imaging applications clinically.^{[51][52]} While higher B_0 fields do result in higher magnetization, it is more difficult to maintain a homogenous field and the costs associated with purchasing and running higher field scanners are much higher.^[57]

In order to create transverse magnetization, the protons in the imaged object are excited by a non-static external magnetic field B_1 applied by transverse RF coils within the MRI scanner.^{[51][52]}

$$B_1 = B_1(t)(\cos(\omega_0 t)i - \sin(\omega_0 t)j) \quad 2 - 4$$

[51][52]

The resulting change in magnetization is expressed in the Bloch equation

$$\frac{d\vec{M}}{dt} = \vec{M}_0 \times \gamma B_1 - \frac{M_x i + M_y j}{T_2} - \frac{(M_z - M_0)k}{T_1} \quad 2 - 5$$

[53]

where i , j , and k are unit vectors in the x , y , and z directions. T_1 is the spin-lattice relaxation constant, and T_2 is the spin-spin relaxation constant, which are inherent properties of material that reflect the time of the return to baseline of the transverse and longitudinal magnetization respectively.^{[51][52]} The signal detected in the transverse coil used to detect the resulting signal, referred to as the receive coil, forms the basis of the MRI signal and resulting image.^[51]

2.2 Relaxation

After perturbation by an external RF field, spins return to their original magnetization through the process of relaxation. In MRI, the return rate of longitudinal magnetization to its original state occurs according to the T1 constant of the imaged substance.^[51] T1 is also referred to as the spin-lattice constant, as the return to baseline magnetization occurs as the deposited RF energy is dissipated into the environment surrounding the spins irrevocably. This process happens exponentially as so

$$M_z(t) = M_0 \left(1 - e^{-\frac{t}{T1}}\right) \quad 2 - 6$$

[51][52]

with the T1 constant being the time for $1 - \frac{1}{e}$ (~63%) of the longitudinal magnetization to return.^{[53][55]}

When full T1 relaxation has occurred, there is no remaining transverse magnetization. However, transverse magnetization can decay faster than this process due to spin-spin relaxation, or T2 relaxation.

This process occurs as

$$M_{xy}(t) = M_{xy}(0)e^{-\frac{t}{T2}} \quad 2 - 7$$

[51][52]

where the T2 constant is the time needed for $\frac{1}{e}$ (~37%) of the transverse signal to remain.^{[53][55]} While T1 relaxation also contributes to the decay of transverse magnetization, there are additional spin interactions occurring within a voxel that cause the net transverse magnetization to decrease, such as spin dephasing or local static field inhomogeneities caused by dipole-dipole interactions of spins in a substance.^[51] In general, pure substances composed of small molecules, like water, have the longest T1 and T2 relaxation times. Field strength affects both constants in a non-linear manner, as the spin-lattice energy dissipation occurs when the molecular tumbling rate of a substance is equal to the Larmor frequency.^[55] T1 is more affected by field strength than T2, and T2 is more affected by field inhomogeneity.^[55]

2.3 Off-resonance

While ^1H protons are the specie of interest in most MRI imaging, other molecular protons exist within the human body, and contribute to the MR signal read by the scanner. As in NMR spectroscopy, these species will precess about the main magnetic field at a Larmor frequency dependent on their inherent gyromagnetic ratio and are referred to as off-resonance spins.^[50,51] A B_1 RF pulse tuned to the Larmor frequency of water ^1H protons will not move spins with a slightly different Larmor frequency into the transverse plane as effectively. In the rotating frame of reference, an on-resonance B_1 RF pulse will move the magnetization into the transverse plane according to the prescribed desired flip angle, α .

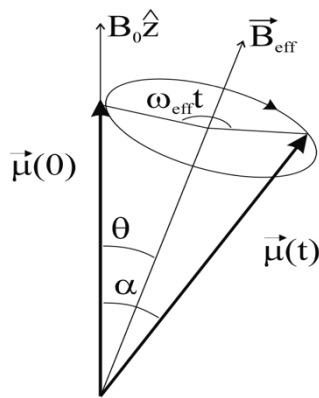


Figure 1: The precession of a magnetic moment around the effective magnetic field in the rotating reference frame
From
Brown, R.W. *et al.* (2014) *Magnetic Resonance Imaging: Physical principles and sequence design*. Hoboken, NJ: Wiley Blackwell.

An off-resonance pulse applied with angular frequency ω_1 to spins with a Larmor frequency of ω would instead have the magnetization precessing about an effective field, \vec{B}_{eff} , as shown in Figure 1, with angular frequency, ω_{eff} , described as

$$\omega_{eff} = \sqrt{(\omega_0 - \omega_1)^2 + \omega_1^2} \quad 2 - 8$$

[50][51][52]

and observed angle from B_0 of

$$\theta = \cos^{-1}\left(\frac{\omega_0 - \omega_1}{\omega_{eff}}\right) \quad 2 - 9$$

[50][51][52]

which results in a smaller transverse magnetization than an on-resonance pulse. This effect is usually deleterious to MR signal and contrast, and various types of off-resonance correction are performed to correct for this issue .^[44,60]

2.4 ³¹P

Phosphorous-31 (³¹P) is another specie of interest in MRS. Its gyromagnetic ratio of $17.235 \frac{\text{MHz}}{\text{T}}$ is only 40% of that of water but is still high enough to achieve acceptable magnetization for MRS.^[54] ³¹P is a stable molecule, with nearly 100% isotopic abundance. Phosphorus makes up around 1% of the total mass of the human body, with 85% of that being in hydroxyapatite within bones. The remaining amount is in various phospholipids and phosphates present in every cell in vital components such as the cell wall, DNA, and Adenosine Triphosphate (ATP).^[59] While the magnetic resonance signal from ³¹P in tissue is much lower than water, it can be detected with dedicated receive coils. ³¹P MRS is best performed under high magnetic fields ($\geq 7\text{T}$) but can be used with certain imaging applications at 3T as well. ^[54] At 3T, the weaker magnetization and low abundance of ³¹P makes it necessary to record non-spatial data with a coil sensing the signal from all the tissue in its range. An example of a ³¹P spectrum is shown in Figure 2, where non-spatial data from the skeletal muscle of a human calf shows the relative abundance of ³¹P species. This method is useful for assessing metabolism, as phosphate groups are exchanged as cellular respiration occurs.^[10,11,33,47,48]

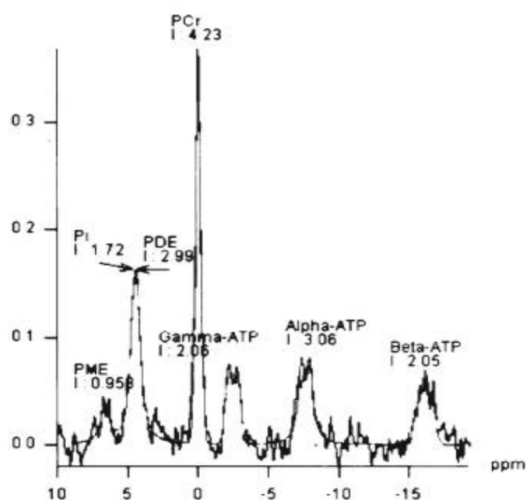
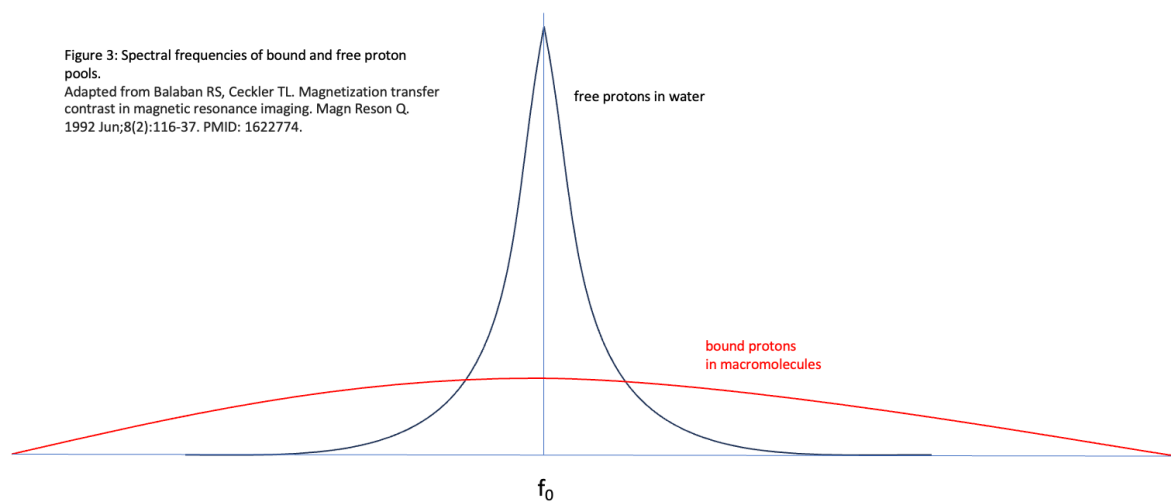


Figure 2: From Isbell 2006, a non-spatial ³¹P spectrum showing relative quantities of phosphorous species in calf skeletal muscle. The PCr peak is largest in this tissue.

2.5 Magnetization Transfer

Macromolecules with bound hydrogen protons with Larmor frequencies far from the center water peak can exhibit a signal lowering effect when imaging tissue.^[67-70] An example of the relative spectral signature of this bound hydrogen pool compared to the free water peak is shown in Figure 3. These bound protons exhibit short T2 decay times due to dipole-dipole interactions and contribute little to the observed MR signal at readout.^[67,68] Water molecules in direct contact with macromolecules exhibit shorter T1 and T2 relaxation rates due to altered molecular tumbling rates as well.^[68,70,71] In addition to these effects, magnetization from the bound proton pool can transfer its magnetization to the magnetically saturated free water pool through the nuclear Overhauser effect (NOE).^[72]



The effect of NOE is shown in Figure 4, where after an on-resonance saturation pulse the bound protein pool will retain most of its longitudinal magnetization due to its broad spectral signature.^[70-72] After a short time, a cross-relaxation will occur between the pools known as magnetization transfer (MT).^[67-70] This leads to less magnetization available in the transverse plane at time of readout, reducing the overall signal from the tissue in the voxel).^[67-70] The MT effect can be used to indirectly image macromolecules that otherwise cannot be seen through MRI. An example of this process is shown in Figure 5, where a broad off-resonance saturation pre-pulse is applied to the macromolecule pool. After MT occurs, there

will be a resulting transverse magnetization reduction at readout. This signal reduction compared to an image with no pre-saturation shows the contribution of macromolecules in each voxel.^[67-71]

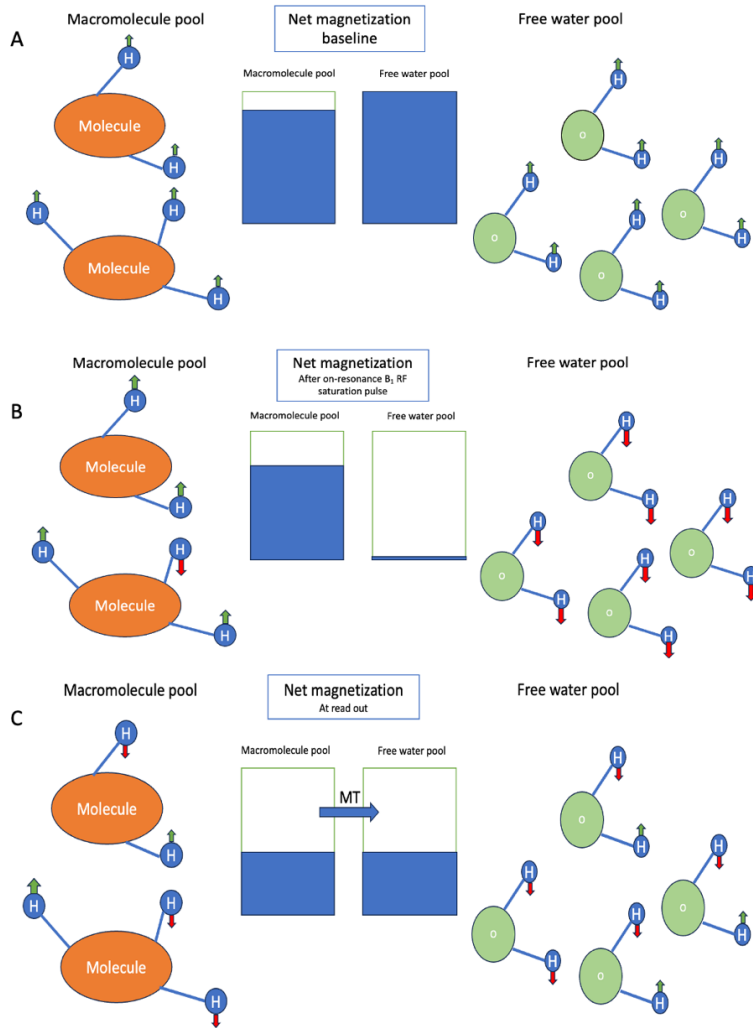


Figure 4: The nuclear Overhauser effect leading to magnetization transfer and its effect on magnetization.

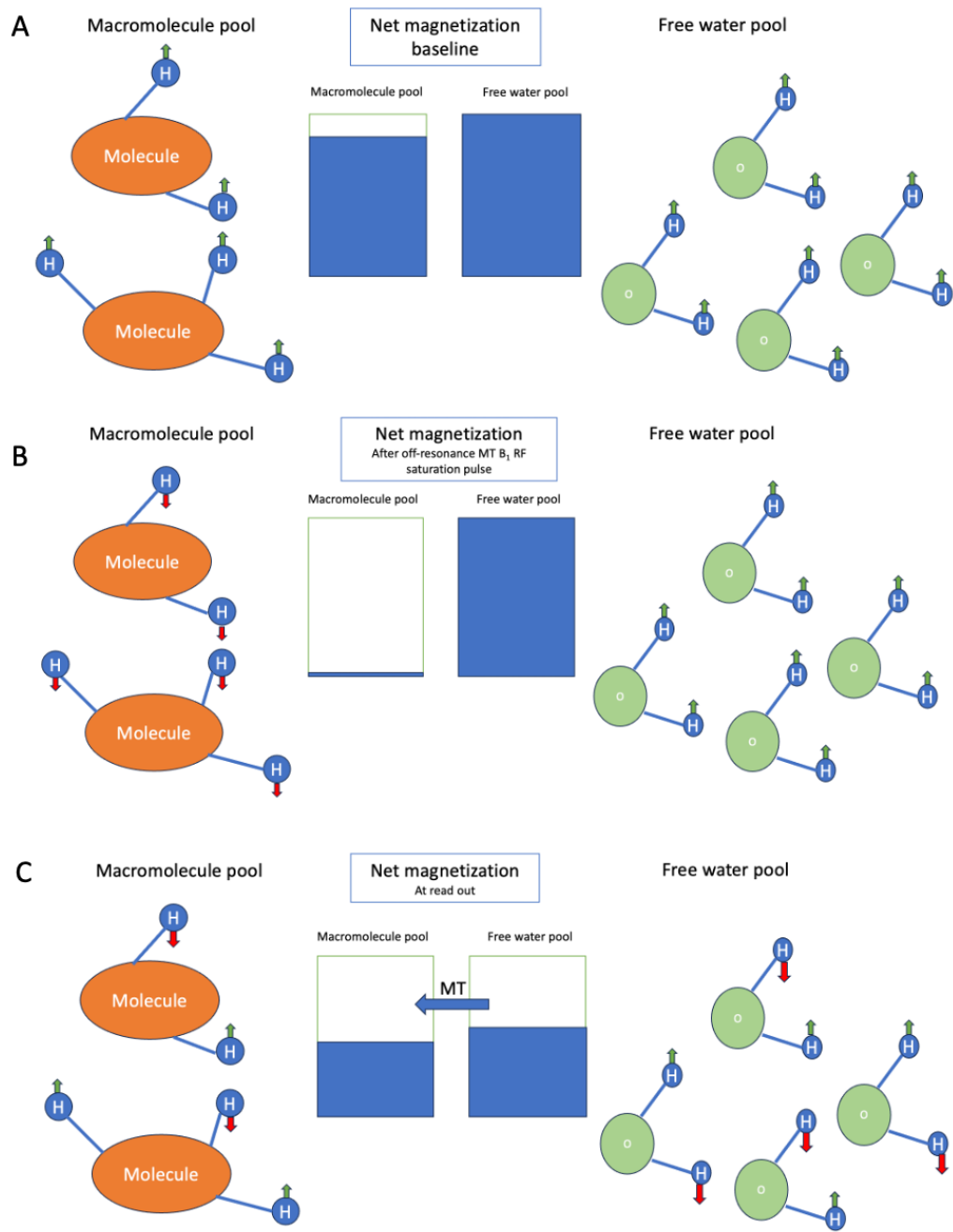


Figure 5: The effect of magnetization transfer imaging preparation pulses on magnetization.

2.6 Chemical Exchange Saturation Transfer (CEST)

A similar effect where magnetization is exchanged between a molecule and free water is chemical exchange saturation transfer (CEST). In contrast to MT, CEST occurs during chemical reactions, like the creatine kinase mediated rephosphorylation of creatine. Figure 6 shows the mitochondrial creatine kinase mediated chemical reaction of creatine and ATP that moves a hydrogen from the amine group of creatine to the free water hydrogen pool.

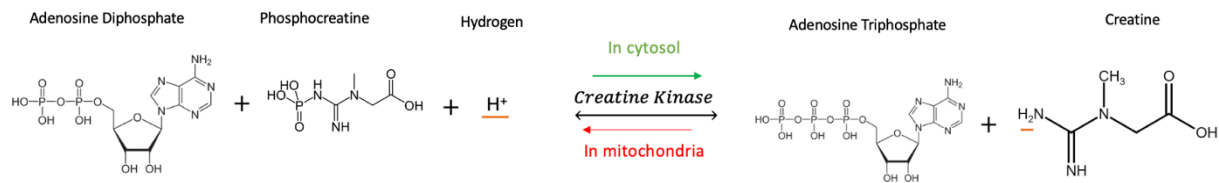


Figure 6: Phosphocreatine metabolism. The hydrogen proton underlined in red joins the amine group of creatine during dephosphorylation.

Figure 7 demonstrates the magnetization exchange that occurs during CEST. The preparation pulse in CEST varies from MT imaging, as the off-resonance target is specific.^[76-79] Figure 8 shows the signal reduction seen when a saturation prep-pulse is given at that frequency plotted along different offset frequencies expressed as parts per million (ppm) away from the center water frequency peak, which is known as a z-spectrum.^[77,78] In our CEST acquisition we sample this curve at six offset frequencies and the center water peak, as shown in Figure 8. From this the CEST signal is the asymmetry ($CEST_{asym}$) between positive and negative offsets as expressed in B-11.^[7,8] The $CEST_{asym}$ should be largest at the offset frequency of the protons being chemically exchanged.

$$CEST_{asym}(\omega) = \frac{S_{-\omega} - S_{\omega}}{S_{-\omega}} \quad B - 11$$

[7,8]

The specific methodology of our CEST sequence is discussed in chapters 3, 4, and 5 of this thesis.

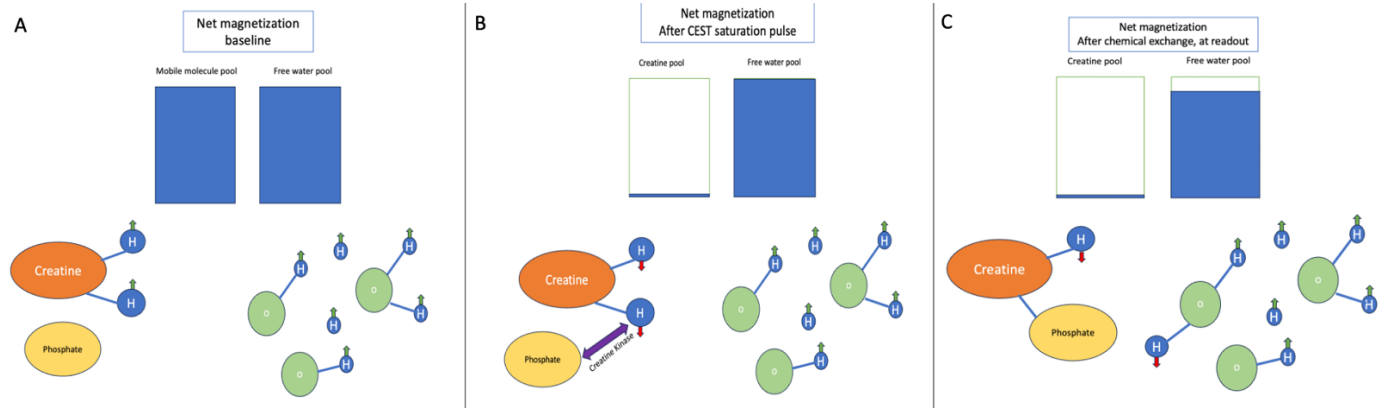


Figure 7: The CEST effect during creatine rephosphorylation and its effect on magnetization

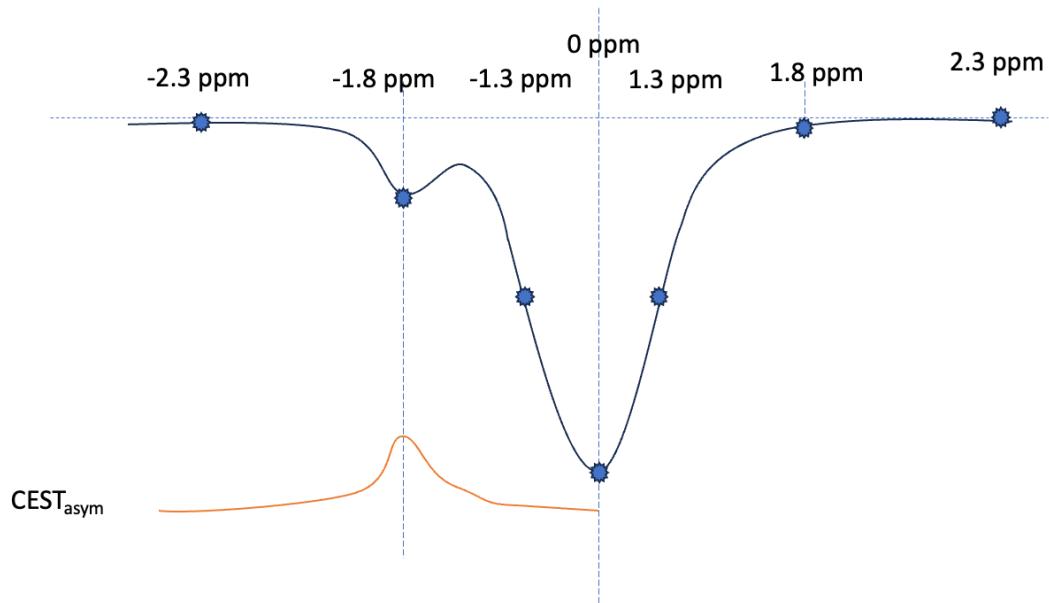


Figure 8: An example of a z-spectrum of creatine rich tissue.

2.7 Phosphocreatine Metabolism

Adenosine triphosphate (ATP) is the main energy source of animal cells, with the energy released from its dephosphorylation allowing non-energetically favorable reactions to occur within the body.^[33] In highly energetic tissue like the skeletal muscles of the limbs there is a need for a secondary phosphorylation system to allow for sustained muscle usage. Phosphocreatine (PCr) along with the enzyme creatine kinase can be used in the cytosol to rephosphorylate ATP and allow for its reuse without cellular respiration occurring.^[31,33] The reaction occurs as shown in Figure 6, with the underlined hydrogen being the targeted exchange proton in creatine CEST.^[7,31] The reverse reaction can only occur within the mitochondria in the presence of oxygen, as shown in Figure 6, or anaerobically in the cytosol through glycolysis generated ATP, the latter of which causes a buildup of lactate in the muscle.^[33,42] Creatine concentration in the muscle will be highest after exercise when phosphocreatine stores are depleted. This concentration decays from peak exponentially under normal conditions within minutes.^[33,42] Without adequate oxygen provided by the microvasculature to the tissue, this concentration will persist longer with only glycolysis available for rephosphorylation.^[31,32,33,42] By the same mechanism, mitochondrial damage will also affect the rephosphorylation of creatine.^[42] Creatine concentration post-exertion thus serves as a useful surrogate for perfusion or mitochondrial health.^[42] Patients with PAD have demonstrated impaired phosphocreatine recovery post-exercise, which is hypothesized to occur due to a combination of acute ischemia and chronic mitochondrial dysfunction.^[10,11,47,48]

2.8 Arterial Spin Labeling (ASL)

MR contrast angiography is a valuable method for assessing blood flow in the lower limbs but is limited by its use of gadolinium-based contrast agents that are contraindicated in patients with poor kidney function and require onsite physician monitoring for their administration.^[4,61] Arterial spin labeling (ASL) is a noninvasive MR method that uses magnetically tagged arterial blood boluses as endogenous

contrast to visualize and quantify perfusion.^[20,63,63] Upstream blood is magnetically inverted before passing into the imaging plane. After a delay to allow for blood travel and perfusion, the slice is imaged, and the tagged blood lowers signal in each voxel present compared to control images. Subtraction images can then be used to calculate quantitative measures of perfusion in terms of flow, usually referred to as cerebral blood flow (CBF) maps in ASL imaging, but in the case of the lower limb we can refer to it similarly as calf blood flow (CBF).^[14,15,62,66] ASL tagging schemas fall into three categories, pulsed (PASL), continuous (CASL), and pseudo-continuous (pCASL).^[20,66] The imaging performing in Chapter 4 of this thesis is a PASL method called Quantitative imaging of perfusion using a single subtraction, second version with thin-slice T_1 periodic saturation (Q2TIPS) with proximal inversion with a control for off-resonance effects (PICORE) tagging. Chapter 5 of this thesis discusses plans to employ a pCASL sequence to improve signal and combine protocols with a CEST sequence.

2.4 Ergometry

Exercise is necessary to observe creatine kinetics, as the metabolic response post ATP and PCr depletion is indicative of mitochondrial health and perfusion.^[33,47,48] Pedal pushing plantarflexion ergometers have been shown to uniformly activate the muscles of the calf, which is a commonly symptomatic area in PAD.^[33,47,48,49] Due to the speed of creatine concentration decay, it is necessary to image as quickly as possible after exercise cessation to properly sample the exponential curve.^[12,13,47,48,49] It is not optimal to have subjects exercise external to the MRI bore, as positioning and localization can take several minutes. Thus, in-bore ergometry best suits the nature of MRI of creatine metabolism, but ergometer design is limited by the size of the bore and ferromagnetic safety concerns.^[49] In our early experiments, ergometry was performed using a plexiglass prototype pedal ergometer, shown in Figure 9, where resistance was provided by a large athletic resistance band. While this low-cost method was useful due to its simplicity and lack of metallic components, it lacked stabilization on the MRI table and did not

have adjustable resistance. Most critically, it interfered with the placement of a multichannel transmit-receive extremity coil.



Figure 9: First stage prototype ergometer

For the data presented in this thesis, ergometry was upgraded to a sophisticated MR-compatible pneumatic pedal ergometer with controllable resistance, the Trispect by Ergospect GmbH.^[49] A diagram of this device is shown in Figure 10. In our experiments, a set exercise length was not successful, as the exercise tolerance between normal subjects and even between PAD varied greatly, as shown in the exercise times in Table 3. Exercise to exhaustion or claudication pain proved to provide a more even relative starting concentration of creatine on CEST images and ^{31}P MRS among subjects, despite being a subjective time depending on subjects' perception.



Figure 10: Schematic of the upgraded ergometer, the Trispect from Ergospect

ASL imaging in the limbs likewise benefits from pre-imaging exercise. Baseline perfusion within the limb provides little ASL signal, so traditionally cuff-occlusion has been used prior to imaging to create hyperemia upon release.^[15,20] Intense exercise can also induce hyperemia sufficient for ASL imaging.^[15] In our studies, plantarflexion ergometry to exhaustion or claudication was used to induce hyperemia, as cuff occlusion can be painful for PAD patients.^[15]

2.5 Peripheral Arterial Disease (PAD)

Atherosclerotic lesions form in vessels of the cardiovascular system in response to stress or damage to vascular endothelium in order to maintain vessel integrity.^[25] A major stressor is the increased shear stress on the intima of the vessel in hypertension leading to damage and inflammation. When this inflammation occurs along with dyslipidemia, this can lead to large low-density lipoprotein laden plaques to form in the intima of the vessel.^[1,26] Oxidative stress from poorly managed diabetes or smoking additionally damages vessel walls and leads to atherosclerosis.^[1,25,26] Large plaques can intermittently block blood flow and tissue perfusion, leading to pain and paresthesia downstream of their location. Plaques that completely occlude a vessel can lead to tissue necrosis or death depending

on the oxidative need of their downstream tissues.^[25] PAD is the term for atherosclerotic disease in the arteries of the limbs. The large arterial vessels that feed the lower limbs, such as the abdominal aorta, iliac, and femoral arteries, are common sites for atherosclerotic plaque formation.^[26] Chronic ischemia can cause pain at rest, numbness, and paralysis. Ultimately, this can lead to ulceration, infection, and tissue necrosis.^[1,26] Within 5 years of a PAD diagnosis around 1-2% of patients will have an amputation and is the leading cause of amputation worldwide.^[1] Among people diagnosed with PAD, around 60% are asymptomatic. Around 30% have pain on exertion that resolves, known as intermittent claudication (IC), and 1-3% have rest pain with or without ulceration, or critical limb ischemia (CLI).^[1] CLI is considered an emergent condition and revascularization is indicated to save the limb.^[21,22] While PAD itself does not directly cause mortality, the exertional pain and decrease of quality of life have devastating effects on patient health. Around 40% of patients die within 5 years of lower limb amputation.^{[27][28]} PAD carries a heavy stigma and mental burden that often leads patients to ignore symptoms and is often comorbid with psychiatric illnesses and exacerbated by socioeconomic health factors.^[29,30]

Diagnosis of PAD relies primarily on the ankle-brachial index (ABI), which is the ratio of systolic pressure at the ankle, divided by the systolic pressure at the arm.^[1,30,31] This is ideally found using a doppler device and blood pressure cuff. As the arm is closer to the heart than the ankle, the blood pressure there should be lower than in the limb in a healthy subject; however, ratios greater than 1.4 can indicate incompressible vessels due to calcification from prolonged oxidative damage.^[1,25,31] A normal value is considered to be 0.9 to 1.4, while less than that is indicative of PAD.^[1] The toe-brachial index (TBI) can be used to assess patients with non-compressible ankle vessels, with a ratio of 0.7 or less considered indicative of PAD; however, this metric has not been as widely verified as the ABI.^[32] While the ABI remains a valuable diagnostic tool, it is not useful in assessing severity of disease, as ABI scores do not correlate with hemodynamic assessments and functional metrics.^[31]

Treatment of non-emergent PAD centers around improving cardiovascular and metabolic health. Statins are a first line treatment of ongoing hyperlipidemia but do little to address existing blockages and vascular damage.^[35] Inhibitors of protein convertase subtilisin kexin type 9 (PCSK9) are highly effective at stopping disease progression and preventing adverse cardiac events but are costly and rarely covered by insurance.^[35,37,39] Likewise, glucose control, smoking cessation, and antihypertensives are recommended to avoid disease progression.^[1,35] Antiplatelet therapies like clopidogrel or low dose aspirin are recommended to inhibit thrombus formation.^[35,39] Cilostazol is a phosphodiesterase III inhibitor recommended for reducing claudication pain and improving walk scores, but has cardiovascular side effects that limit its clinical utility.^[35,39] Supervised exercise remains the treatment option with the highest level of evidence for stopping disease progression and improving quality of life, but requires painful exercise and patient compliance.^[36,41]

Revascularization

Patients with severe CLI can progress to having chronic limb threatening ischemia (CLTI), where a substantial amount of blood flow is obstructed, causing pain at rest and risk of gangrene.^[21]

Revascularization procedures are performed on patients with CLTI to restore blood flow to tissue downstream of occluded arteries. Surgical revascularization methods employ venous bypass grafting to create an alternative flow path around occlusions in the major arteries of the leg.^[21] Endovascular revascularization uses transluminal devices such as balloons or stents to perform angioplasty. The inflated balloon or placed stent widens the lumen of the vessel, and can also elute anti-proliferative drugs.^[21,22] Both methods have similar patient outcomes, with more than 40% experiencing major adverse limb events or death within five years of the procedure.^[21,22] The goal of these procedures in CLTI is primarily limb salvage, while their use in IC is more focused on reducing symptoms and improving quality of life.^[38,39] There is little evidence to support the use of revascularization for IC patients, with some studies suggesting it may exacerbate symptoms or worsen outcomes.^[31,40,41] The ABI increase seen

after revascularization is indicative of the success of the procedure in restoring blood flow, but does not correlate with functional improvements or long term limb outcomes.^[31,38,40,41]

Hypoxia and Nitrate

Vasodilation has an ameliorative effect on PAD by expanding narrowed vessel diameters and reducing hypertension.^[39,43] Nitric oxide (NO) induces smooth muscle relaxation in the vasculature through increasing cyclic guanosine monophosphate (cGMP), a signaling molecule.^[45] Inorganic nitrate consumption has been shown to increase plasma NO levels and provide symptomatic relief in PAD patients with claudication pain.^[23,24,43] In addition to its vasodilatory effect, NO is hypothesized to increase mitochondrial efficiency by reducing the expression of adenine nucleotide translocase (ANT), which speeds the process of exchanging ADP and ATP across the inner mitochondrial membrane.^[76] NO is protective against mitochondrial damage in hypoxia by reducing free radical formation from the electron transport chain in the absence of oxygen.^[73] NO also increases the expression and binding activity of hypoxia inducible factor 1- α (HIF1 α).^[74,75] HIF1 α is expressed in response to hypoxic conditions and helps facilitate adaptations, like collateral vessel formation and muscle fiber type changes to accommodate more glycolytic metabolism.^[74,75] These combined mechanisms present inorganic nitrate supplementation as an attractive treatment for PAD.

Chapter 3: CrCEST method can distinguish creatine kinetics in PAD patients compared to age matched controls

3.1 Rationale

We hypothesize that ischemia in PAD leads to altered creatine concentration decay post-exercise in patients compared to age-matched controls. The effects of PAD on creatine metabolism are not fully understood, but prior studies with ³¹P MRS show an observable and repeatable difference in metabolism for PAD patients.^[6] We also aimed to test the ability of CrCEST to do so on a muscle group basis. Subjects performed plantarflexion ergometry to exhaustion or claudication using a calf ergometer that is capable

of uniformly activating the calf muscles. The comparison of the two methods shows the utility of CrCEST in the study of PAD energetics.

3.2 Methods

Patients between the ages of 35 to 85 years with symptoms of intermittent claudication or critical limb ischemia and a documented ankle brachial index (ABI) of <0.9 were eligible for this study. Exclusion criteria included lower extremity vascular surgery or percutaneous intervention <3 months prior to enrollment, gangrene, or a non-healing wound in the foot of the leg of interest, need for urgent revascularization, active coronary artery disease or recent (<2 months) myocardial infarction, body mass index of >40 , or a known contraindication to MRI. Normal human subjects without risk factors for atherosclerosis were recruited from the community to serve as age-matched control subjects. Subjects with risk factors were eligible only with normal ABIs. The protocol was approved by the Human Investigation Committee at the University of Virginia, and all participants signed informed consent. CMK had access to all data and takes responsibility for its integrity and the data analysis.

CrCEST images were obtained on a 3T MRI scanner (Prisma, Siemens Medical Solutions, Erlangen, Germany) using a 15-channel transmit-receive extremity coil centered at mid-calf. Creatine level measurements were acquired using a pulse sequence developed at University of Pennsylvania.^[8, 9] Water saturation shift referencing (WASSR) and B1 maps were collected for B0 and B1 correction, respectively.^[44] Six images were acquired over 24 s intervals with saturation frequency offsets of ± 1.3 , ± 1.8 , and ± 2.3 ppm. The CEST effect reduces the signal at $+1.8$ ppm compared to the reference at -1.8 ppm, with this asymmetry quantified as $CEST_{asym}$. A 500ms saturation pulse train was applied consisting of five 99.6ms Hanning-windowed pulses with 150 Hz peak B1 amplitude and 0.4ms inter-pulse delay. Imaging parameters were single-shot spoiled gradient-echo readouts with centric encoding, fat saturation, flip angle 10° , field of view (FOV) 160x160 mm, matrix 144x144, in-plane resolution 1.1 mm, repetition time (TR) 6.0ms, echo time (TE) 2.9ms, and slice thickness 10 mm.

Subjects were placed supine, feet first, into the scanner, with the foot of the leg of interest placed in an MR-compatible plantar flexion ergometer (Trispect, Ergospect GmbH, Innsbruck, Austria). A reference image and B1, B0, and WASSR maps were collected.^[44] This was followed by 4 baseline CrCEST images obtained prior to exercise.^[9] Then subjects were asked to begin plantarflexion in time with a metronome set at 60 bpm until claudication symptoms or calf exhaustion. This was chosen to ensure all subjects reached a state of muscle ischemia. The ergometer resistance was adjusted for the subjects' ability to pedal uniformly against the resistance level. Immediately post exercise, 25 images were obtained. This was followed by repeat B0, B1, and WASSR maps.^[44] Five subjects in each group returned for studies of test-retest reliability.

Studies were analyzed blinded to subject group. Creatine concentration decay times were generated from ROIs including the entirety of the tibialis anterior, posterior compartment, gastrocnemius, and the whole calf (excluding bones) for each subject in MATLAB (MathWorks, Natick, Massachusetts). The soleus muscle was not included in analysis, as it is not activated as uniformly as the other muscles during plantarflexion, and it contains several large vessels that are difficult to exclude during analysis. Decay times were generated from the individual ROIs and recorded for each subject (Figures 11 and 12).

For ³¹P MRS studies, subjects were positioned in the scanner with the same foot on the ergometer pedal with a multinuclear surface coil against their gastrocnemius muscle, and 5 pre-exercise spectra were acquired. After subjects performed plantar flexor ergometry to claudication or calf exhaustion, 25 signal averages were acquired after 4 preparation pulses at a repetition time of 550 ms for a total acquisition time of 16 s per spectrum, and 18 spectra were acquired at the cessation of exercise.^[6]

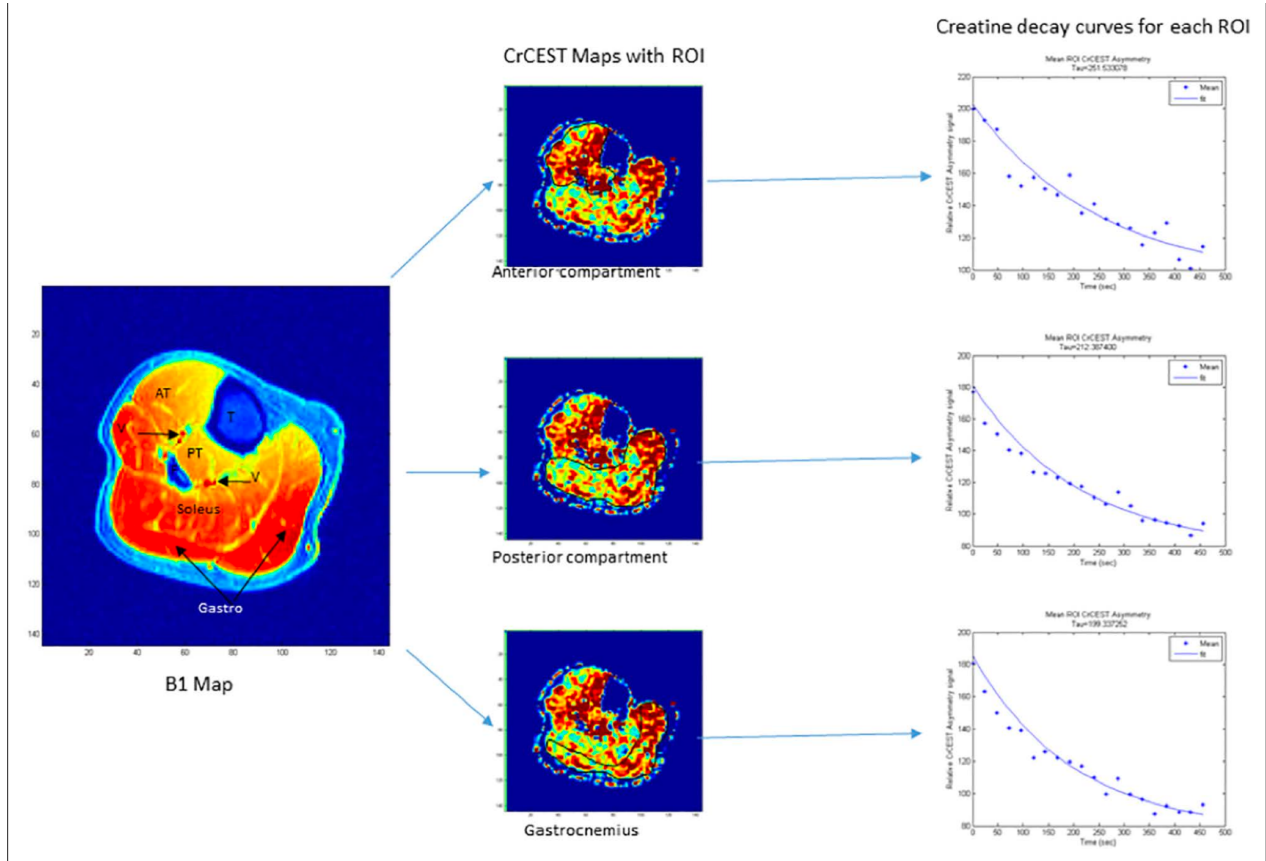


Figure 11: Calf muscle maps, chemical exchange saturation transfer asymmetry maps, and regions of interest with decay curves. AT indicates anterior tibialis m.; CrCEST, chemical exchange saturation transfer of creatine; F, fibula; Gastro, gastrocnemius m.; PT, posterior tibialis m.; ROI, region of interest; Soleus, Soleus m.; V, arterial and venous vessels; and T, Tibia.

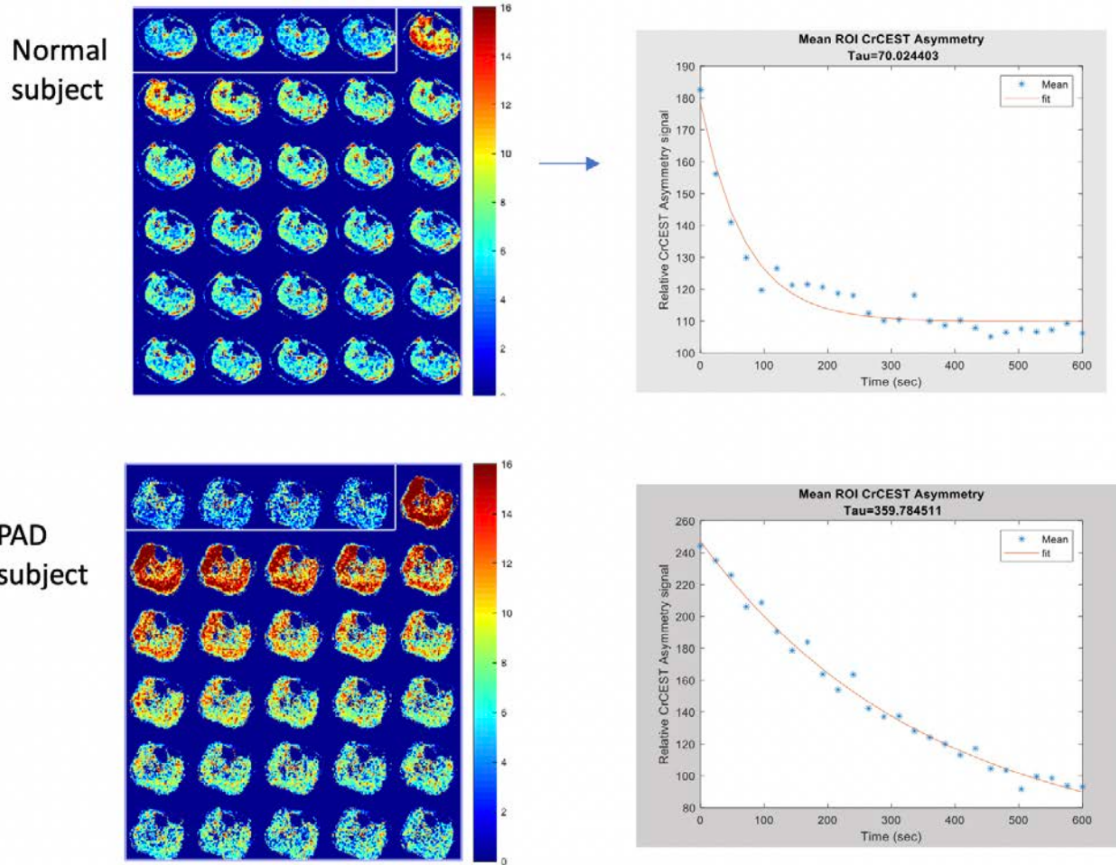


Figure 12: Example chemical exchange saturation transfer (CEST) images and corresponding CEST asymmetry ($CEST_{asym}$) decay curves from a normal control (top) and a patient with peripheral artery disease (PAD). The first 4 images are pre-exercise, and the subsequent images begin immediately post-exercise. Note the red color depicting increased $CEST_{asym}$ signal immediately post-exercise that resolves quickly in the normal subject and takes significantly longer to normalize in the PAD subject. This is reflected in the much longer $CEST_{asym}$ decay constant in the patient with PAD (bottom right). CrCEST indicates chemical exchange saturation transfer of creatine; and ROI, region of interest.

Statistical Analysis

Subject characteristics were summarized as mean and standard deviation for continuous variables and by frequencies for other variables. Characteristics were compared between control subjects and patients using the Student t-test or Wilcoxon rank-sum test for continuous variables and the Pearson χ^2 test or Fisher exact test for categorical variables. Exercise times and $CEST_{asym}$ decay were summarized as median and interquartile range (IQR). Pearson correlation coefficients were calculated for $CEST_{asym}$ decay

times after log transformation compared with demographic variables. Pearson correlation was performed comparing CEST decay constant and phosphocreatine recovery time constant. For all comparisons, $P < 0.05$ was considered significant. Agreement between phosphocreatine recovery by ^{31}P MRS and $\text{CEST}_{\text{asym}}$ decay was analyzed using the method of Bland and Altman. Test-retest reliability for $\text{CEST}_{\text{asym}}$ decay was also analyzed in 5 subjects who underwent testing twice at different time points using Bland-Altman. Analysis was performed using SAS, version 9.4 (SAS Institute, Cary, NC).

Table 1: Demographics of the Study Population

	Controls	PAD	<i>P</i> value*
Number of subjects, n	29	35	...
Women, n (%)	17 (59)	4 (11)	<0.001
Black, n (%)	1 (3)	7 (20)	0.063
Mean age, y; mean \pm SD	65 \pm 8	66 \pm 8	0.103
Diabetes, n (%)	3 (10)	14 (30)	0.007
Hypertension, n (%)	5 (17)	29 (83)	<0.001
Hyperlipidemia, n (%)	7 (24)	30 (86)	<0.001
Coronary artery disease, n (%)	4 (14)	13 (37)	0.035
Smoking, n (%)	2 (7)	31 (89)	<0.001
ABI of leg studied, mean \pm SD	...	0.65 \pm 0.11	...

ABI indicates ankle brachial index; and PAD, peripheral artery disease.

**P* value was generated by using the Pearson χ^2 test or Fisher exact test for categorical variables, and the Student *t* test for normally distributed continuous variables.

3.3 Results

A total of 64 subjects were studied; 35 subjects with PAD and 29 controls. The mean age was similar between groups (Table 1), but there were fewer women in the PAD group. The mean ABI for the PAD group was 0.65 ± 0.11 . Demographics are shown in Table 1. A majority of patients with PAD had at least one of the following conditions: hypertension, hyperlipidemia, or a smoking history. Approximately one-third of patients with PAD had coronary artery disease. Very few of the normal subjects had risk factors for atherosclerosis. Plantar flexion exercise times tended to be longer in the normal subjects as would be expected, but this difference did not reach statistical significance due to the wide variation in exercise times in both groups (Table 2). The $\text{CEST}_{\text{asym}}$ decay times for the overall calf as well as the individual gastrocnemius and posterior tibialis in the PAD group were increased compared with the age-matched control group (Table 2). $\text{CEST}_{\text{asym}}$ decay times were similar between groups in the anterior tibialis. The $\text{CEST}_{\text{asym}}$ levels at end-exercise was $178 \pm 58\%$ of baseline in PAD subjects and $180 \pm 33\%$ of baseline in control subjects, $P=0.86$. A history of hypertension was associated with prolonged whole calf $\text{CEST}_{\text{asym}}$ decay times in the entire group of 64 subjects ($r=0.32$, $P<0.01$) as was history of smoking ($r=0.26$, $P<0.04$). There was no association between ABI and $\text{CEST}_{\text{asym}}$ decay times. Age tended to be associated with the $\text{CEST}_{\text{asym}}$ decay times in the anterior tibialis ($r=0.24$, $P<0.06$), but not in other muscle groups. A history of CAD was associated with $\text{CEST}_{\text{asym}}$ decay times in the anterior tibialis ($r=0.30$, $P<0.02$) and posterior tibialis ($r=0.32$, $P<0.01$). Test-retest reliability was performed on 5 normal subjects and 5 patients with PAD. Measurements were obtained at a mean time of 1 ± 1 days after the initial scan. Exercise times for the 10 subjects were similar between the 2 time points (168 ± 137 s at time 1 and 246 ± 287 s at time 2, $P=0.45$). Results for agreement are displayed using Bland-Altman analysis (Figure 13) showing very good agreement with 1 data point lying outside the 2 standard deviations. Thirteen patients with PAD and 11 normal patients were imaged by CEST and underwent ^{31}P MRS,

where observed pH at end-exercise was not different between groups (7.02 ± 0.05 in PAD and 7.07 ± 0.08 in controls, $P=NS$). Table 3 demonstrates the data from these studies. Figure 14 displays the Bland-Altman analysis between the 2 groups showing good agreement. Figure 15 shows a Pearson correlation plot showing 3 patients with high phosphocreatine recovery time constant yet relatively preserved CEST decay and resultant lack of correlation.

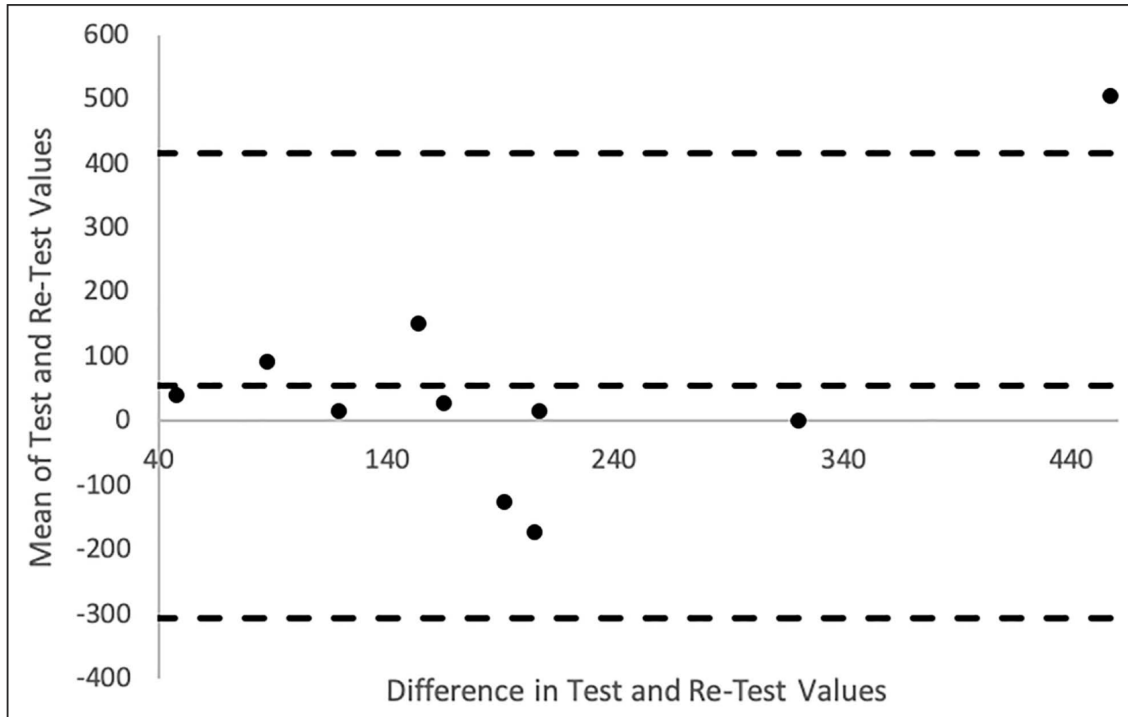


Figure 13: Bland-Altman plot comparing test-retest values in a total of 10 subjects (5 with peripheral artery disease and 5 controls). There is one data point that does not lie within 2 SDs of the difference between the 2 studies.

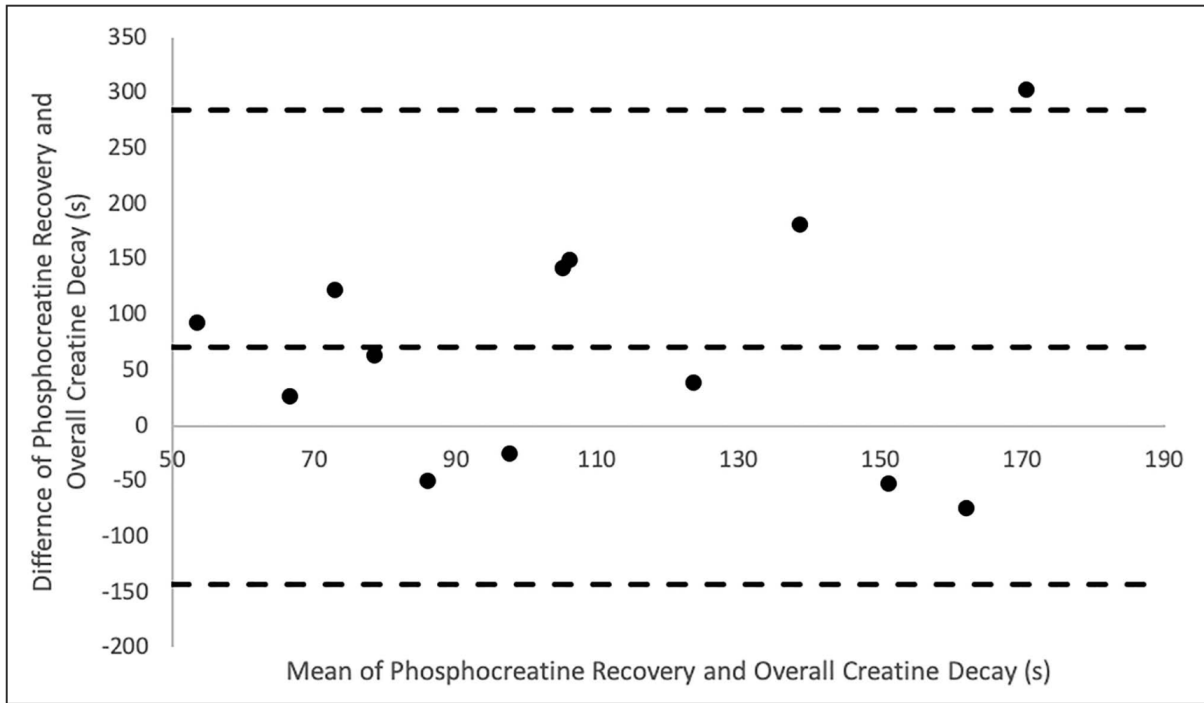


Figure 14: Bland-Altman plot comparing PCr recovery time constant by ^{31}P MRS and $\text{CEST}_{\text{asym}}$ decay constant for 13 patients with peripheral artery disease and 11 normal controls. Agreement is excellent.

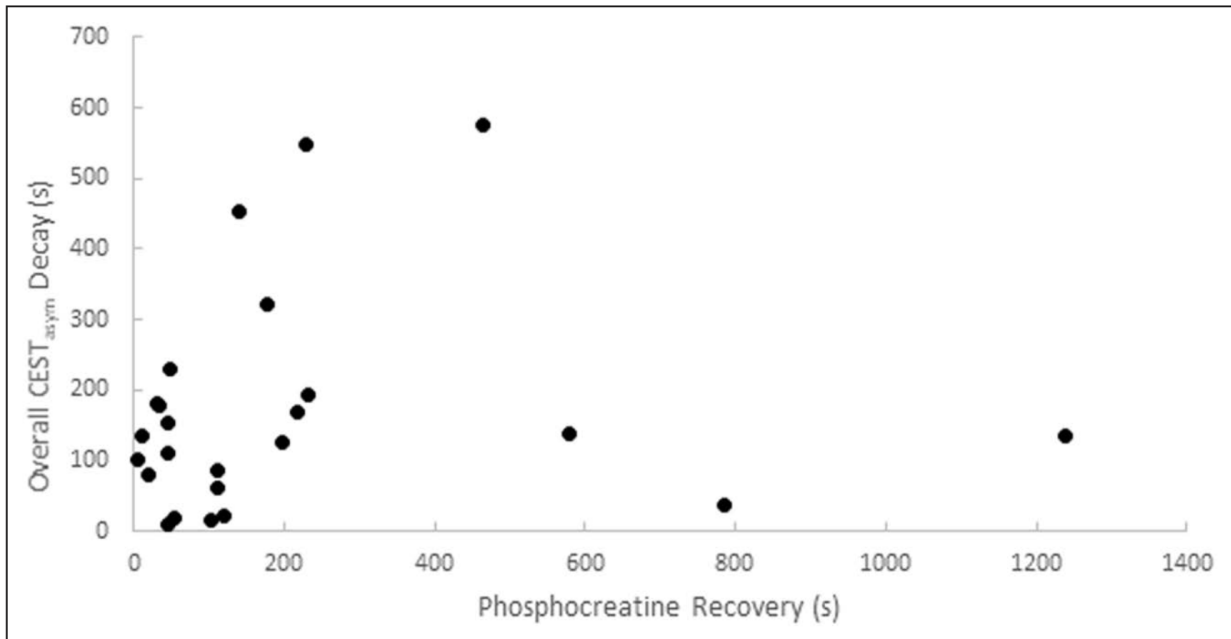


Figure 15: Pearson correlation plot of chemical exchange saturation transfer (CEST) decay constant versus phosphocreatine recovery time constant. $P=0.66$, $r=0.09$.

Table 2: CEST_{asym} Results

	Controls, n=29	PAD, n=35	P value
Exercise time (s), median (IQR)	251 (538)	125 (87)	0.19
Calf CEST _{asym} decay constant (s), median (IQR)	152 (84)	276 (329)	<0.03
Tibialis anterior CEST _{asym} decay constant (s), median (IQR)	126 (182)	139 (246)	0.36
Tibialis posterior CEST _{asym} decay constant (s), median (IQR)	125 (142)	186 (347)	<0.02
Gastrocnemius CEST _{asym} decay constant (s), median (IQR)	178 (127)	267 (300)	<0.03

CEST_{asym} indicates chemical exchange saturation transfer asymmetry; IQR, interquartile range; and PAD, peripheral artery disease.

Table 3. Data From PAD and Controls Undergoing Both CEST and ³¹P MRS Post Exercise

	Controls, N=11	PAD, N=13	P value*
Exercise time, s; median (IQR)	224 (450)	125 (199)	0.192
Calf CEST _{asym} decay constant, s; median (IQR)	134 (115)	134 (330)	0.524
Phosphocreatine recovery time constant, s; median (IQR)	46 (80)	199 (492)	0.007

CEST_{asym} indicates chemical exchange saturation transfer asymmetry; IQR, interquartile range; MRS, magnetic resonance spectroscopy; and PAD, peripheral artery disease.

*P value was generated using the Wilcoxon rank-sum test for non-normally distributed continuous variables.

3.4 Discussion

This study examined differences in creatine kinetics between normal subjects and patients with PAD using CrCEST-based MRI. We found that patients with PAD demonstrated a significant increase in creatine decay times in the entire calf compared to their normal age-matched controls. In addition, the difference in creatine decay was also able to be isolated to the specific muscle groups of the calf including the gastrocnemius and posterior tibialis muscles. When compared with normal subjects, there was an almost two-fold increase in the creatine decay time in PAD patients. This is the inverse of the increase in phosphocreatine recovery times seen in the patients who underwent ^{31}P -MRS in our previous studies. However, the ability to isolate specific muscle groups is an advantage of CrCEST compared to ^{31}P -MRS and raises the potential for utilizing this technique to evaluate therapies that might improve perfusion in specific muscle groups. These results indicate that CrCEST can be used to differentiate creatine kinetics in PAD and normal patients with excellent spatial resolution. Test-retest reliability of the CrCEST decay measures was very good.

Measuring tissue energetics in exercising skeletal muscle in PAD has been performed with ^{31}P MRS for over 25 years.^[10] Chronic limitations in blood flow can lead to maladaptive changes within mitochondria that lead to delayed phosphocreatine recovery, although there is not a direct correlation between perfusion and energetics in the later stages of PAD.^[6,11] The present study significantly extends prior studies using the relatively new CrCEST technique which were primarily aimed at proof of concept. For example, prior studies were performed with few subjects ($n = 3$ PAD patients and 3 controls) and one study showing reasonable agreement between CrCEST and ^{31}P -MRS was performed in only 6 volunteers, not in PAD.^[7,8] Feasibility and reproducibility of these measurements has been shown, again with small numbers of volunteers, at higher field strength (7T).^[12] The present study sets the stage for clinical applications of the technique.

A major challenge for the development of new therapies in PAD is the lack of quantitative measures for measuring tissue physiology such as energetics and perfusion. Large vessel inflow as measured by ABI and angiography does not reflect the tissue effects of therapies. CrCEST offers such promise as an attractive target for assessing benefits of revascularization, other novel therapies, and clinical outcomes in PAD. ^{31}P MRS has been available since the 1980's for evaluation of PAD but has not been utilized clinically due in part to lack of availability due to lack of multi-spectral capabilities at many centers. Strengths of ^{31}P MRS include the extensive literature supporting its application in PAD, its reproducibility, and robustness. CrCEST is an imaging technique that does not require multispectral hardware and thus could theoretically be applied on any high field clinical scanner with the appropriate pulse sequence and thus has far broader clinical potential than ^{31}P -MRS. In addition, the ability to localize abnormal energetics to individual muscle groups could allow the development of vessel and thus muscle-specific revascularization therapies.

Differences between PAD subjects and controls were seen in each muscle group except for the anterior tibialis. The anterior tibialis muscle contains more fast twitch muscle fibers than the rest of the calf, allowing it to function better in hypoxic conditions.^[13] This may account for the similar results between groups. In addition, plantar flexion exercise appears to trigger preferential use and higher perfusion of the anterior tibialis¹⁴ and this may also account for less of a difference between PAD and normal subjects. Hypertension and a history of smoking were associated with prolonged CrCEST decay times. Future studies may determine the mechanisms underlying these risk factors effects on calf muscle energetics and whether reduced perfusion plays a role.

Our group has developed novel non-contrast methods of measuring tissue perfusion in PAD subjects using arterial spin labeling (ASL) MRI after exercise or with thigh cuff occlusion/hyperemia.^[14,15]

Similarly to CrCEST, perfusion can be measured by ASL on a per muscle group basis. Combining these non-contrast measures of perfusion and energetics could offer significant potential for understanding

the physiologic effects of revascularization and novel medical therapies on specific muscle groups in the calf. Perfusion as measured with single photon emission tomographic techniques has been shown to be an important marker of prognosis, predicting amputation-free survival in PAD.^[16] Future studies will help determine whether perfusion, energetics, or the combination are the best predictors of PAD outcome.

3.5 Limitations

Gender differences could in theory account for the differences in creatine decay between normal and PAD patients as there was a significantly higher number of women in the normal group. In addition, the present study did not include patients with non-compressible vessels with ABIs >1.3 that may have symptoms of PAD. CrCEST decay times are significantly longer than PCr recovery time constant. Based on chemical principles, the rate of creatine decay should parallel phosphocreatine recovery. However, ³¹P MRS is not spatially localized and thus is likely preferentially measuring gastrocnemius energetics due to the location of the ³¹P surface coil. As shown in Table 2, gastrocnemius decay times appear to be somewhat longer than other muscle groups and this may account for some of the difference. Additionally, at 3T the resulting CEST_{asym} signal likely receives interference from tissue acidification, particularly lactic acid buildup from anaerobic muscle metabolism due to ischemia.¹⁷ Other potential reasons for the longer CrCEST decay include signal to noise issues, patient motion, nonlinearity, or relative insensitivity to creatine levels from a technical standpoint. A major advantage ³¹P has over this fast time-course CrCEST is that relative quantities of phosphorous metabolites (ATP, PCr, Pi and pH) can be imaged at once. Doing so using ¹H CEST would require finely sampling the z-spectra through multiple excitations, making the resulting time-course too long to assess kinetics. In addition, CrCEST and ³¹P-MRS are dependent on mitochondrial function, which has shown to be altered in patients with heart failure.^[18] As many patients with PAD have some degree of CAD and may have resultant reduced left ventricular function, there is a risk for confounding due to this. However, the

PAD cohort in this study had a mean ejection fraction of $60\% \pm 4\%$ with only one patient having a clinical diagnosis of heart failure, so it is unlikely that heart failure is contributing significantly.

Lastly, with regards to the technique itself, one of the difficulties is high sensitivity to patient motion during scanning. The patients were instructed to lie as still as possible in the scanner during imaging.

Another potential difficulty is with fitting the creatine decay curves as they may be altered due to combination of abnormal creatine kinetics, motion artifact, and interference from vessel and bony structures when drawing regions of interest. Given its size relative to other muscles in the calf, the gastrocnemius muscle is the easiest to identify on the CEST maps, and therefore, the most consistent to draw the ROI. This may explain, in part, why it demonstrated the greatest difference in creatine decay between the PAD patients and normal subjects. Next steps will include correlation of energetics as measured with CrCEST with muscle-specific perfusion as measured by ASL in PAD patients. Longer term studies that follow PAD progression will be useful in showing CrCEST energetics' ability to predict patient outcomes.

Chapter 4: MRI methods to study the relationship of changes in perfusion and energetics with revascularization in PAD

4.1 Rationale: Surgical and endovascular revascularization procedures are considered first-line treatments for moderate to severe PAD in order to restore blood perfusion to the affected limb. We studied the metabolic changes in PAD patients before and after revascularization procedures and tracked patients who do not receive procedures or take inorganic supplements to manage their disease. Patients with Intermittent claudication (IC) have PAD symptoms that resolve during rest, while critical limb ischemia (CLI) is a subset of severe PAD that presents with pain at rest, ulceration, or gangrene. This progression occurs in about 25 percent of PAD patients within 5 years of diagnosis and is typically associated with an ABI of <0.4 but can occur at higher ABIs as well.^[1] Patients with either type of PAD may be candidates for a revascularization procedure, but CLI is considered an emergent condition where

revascularization is necessary to preserve the limb. Arterial spin labeling (ASL) uses tagged inverted arterial blood as endogenous contrast to visualize and quantify perfusion into tissue. Combining ASL and CrCEST in the same protocol allows for spatial visualization of metabolism and perfusion. The goal of this study was to use this combination to assess changes after revascularization in patients undergoing both endovascular and surgical procedures and evaluate the recovery of both perfusion and metabolism in their muscle tissue. Additionally, we assessed patients that were not planning on having revascularization. This arm included a sub-study where subjects received beetroot juice supplementation to study the effect of dietary inorganic nitrate on PAD. We recruited 19 patients, 11 of which had revascularization procedures.

4.2 Methods: All subjects underwent an MRI on a 3T PRISMA Siemens scanner using a transmit-receive knee coil. All subjects underwent baseline imaging in which water saturation with shift reference (WASSR) and B1 maps were collected for B0 and B1 correction.^[7,44] Six images were then acquired over 24 second intervals with saturation frequency offsets of ± 1.3 , ± 1.8 , and ± 2.3 ppm. The CEST effect reduces the signal at +1.8 ppm compared to -1.8 ppm, referred to as CrCEST_{asym}. Subjects performed plantarflexion ergometry on an MR-compatible ergometer (Ergospect, NL) until calf exhaustion at which point post-exercise images were obtained. CrCEST_{asym} maps were obtained with a region of interest (ROI) drawn around the anterior tibialis, posterior tibialis, and gastrocnemius muscles. Creatine decay times were obtained by fitting an exponential curve to the CrCEST_{asym} values. For the ASL imaging, control-tagged image pairs were acquired repetitively using a PASL pulse sequence. The tag was applied 35 mm proximal to the first imaging slice for 1200 ms, followed by a 1500 ms post-label delay^[14] The delay is needed to ensure that the entire bolus reaches the distal slice before imaging, thus avoiding potential underestimation of blood flow.^[19, 20] Motion correction was performed between temporal frames and relative blood flow maps using a simplified single compartment ASL model.^[14,15] ROI were drawn around the muscle group demonstrating the highest perfusion and compared to the

corresponding muscle group. Ten subjects (62.1 ± 9.9 years) with known PAD (defined as symptoms of claudication with confirmed ankle-brachial index < 0.9) scheduled for revascularization were enrolled. Eleven subjects not undergoing procedures were also enrolled, six with no intervention, and five under a double-blinded study of inorganic nitrate supplementation in PAD. The structure of the recruitment arms is shown in Figure 16. Due to low recruitment numbers, the recruitment arms were collapsed for analysis as shown in Figure 17.

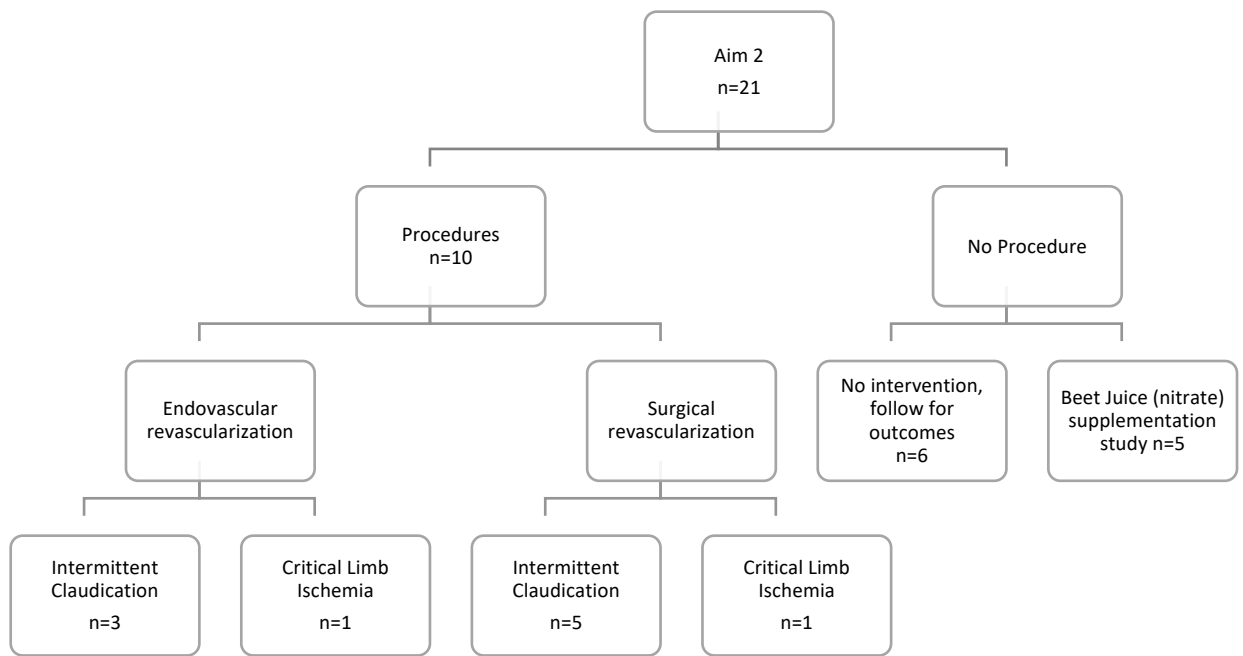


Figure 16: Total patient recruitment arm structure

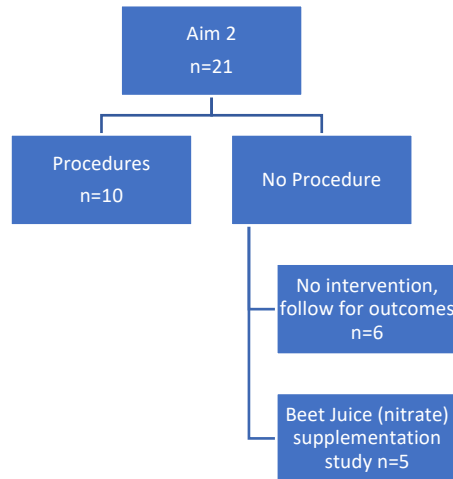


Figure 17: Collapsed recruitment arm structure

All recruitment arms had at least one scanning session with CrCEST and ASL data collected, and a 6-minute walk score performed. Patients in the procedures arm were imaged before revascularization, and at both 6 weeks and 6 months after their procedure. 6-minute walk scores and new ABI readings were also taken at each time point to compare the effects on bulk perfusion and functionality. Patients in the no procedure, no intervention arm were scanned once, but their limb and health outcomes were tracked for changes. The beetroot juice supplementation testing was a double-blind, randomized, crossover design.²⁴ Five male patients (72.2 ± 5.2 years) with symptomatic PAD underwent resting blood draw and a symptom limited cardiopulmonary treadmill exercise test. Health characteristics on these subjects is shown in Table 6. On a separate day, plantar flexion exercise was performed until claudication symptoms using the same MR-compatible ergometer. CEST and ASL imaging was performed using the same protocol as the procedure subjects immediately at the cessation of exercise. All subjects consumed ~5 days of 13 mmol NO_3^- supplementation or identical NO_3^- -depleted placebo before each treadmill and MRI test. This was repeated two weeks following with either the placebo or nitrate-rich beetroot juice depending on their initial assignment. Six patients either denying or ineligible for

revascularization had one visit with the same imaging protocol and had their electronic medical records tracked for cardiovascular and limb outcomes.

4.3 Statistical Analysis:

Intrasubject changes in ABI, CrCEST decay, ASL flow, and 6-minute walk score at 6 weeks and 6 months were compared to baseline using a paired one tailed t-test with 95% confidence intervals. CrCEST data from each muscle group was correlated to flow measurements from corresponding muscle groups using Pearson's correlation coefficient at each time point. ASL and CrCEST was also compared to the 6-minute walk score using Pearson's correlation coefficient.

4.4 Results:

Ten PAD patients were imaged before and after revascularization. Due to COVID-19 pandemic precautions, follow-up imaging was problematic for some patients. Data from a patient who returned at all time points is shown in Figure 18. This patient underwent a posterior approach to left popliteal-popliteal bypass using reversed great saphenous vein, after which the ABI was improved from 0.71 to 1.12. The ASL perfusion shows an increase in flow to the gastrocnemius, with a restriction of flow to the rest of the muscle groups at 6-weeks, that becomes a uniform increase throughout the calf at 6-months. The tau time-constant of the CrCEST decay initially elongates at 6-weeks post revascularization, where the six-minute walk score also worsens. At 6-months the decay shortens, and the walk score improves. Table 4 shows ABI, CEST, ASL, and 6-minute walk score changes post-revascularization. The changes in ABI, 6-minute walk score, and ASL (except the anterior tibialis at 6 weeks) were found to be statistically significant, while none of the CEST groups were. Table 5 shows the Pearson's correlation coefficient between ABI, CEST, ASL, and 6-min walk score for the revascularization group. None of these data were significantly correlated besides ABI and 6-min walk score before procedure and higher AT ASL signal was negatively correlated with six-minute walk score at 6 weeks.

In the beet root supplementation group, following beetroot juice supplementation, plasma nitrite (NO_2^-) concentration increased significantly compared to placebo (410.5 ± 237.5 v 156.3 ± 45.4 nM; $p < 0.01$). There was a trend towards longer pain-free walking with subjects walking 30% longer following beetroot juice supplementation (312.8 ± 207.3 vs 238.5 ± 197.8 sec; Cohen's $d = 0.37$) with no change in peak walking time (585.8 ± 56 vs 589.5 ± 103.6 sec; $p=0.94$). Nitrate also tended to demonstrate higher tissue perfusion at peak plantar flexion exercise (32% increase; 22.9 ± 17.4 vs 17.4 ± 10.5 mL/min/100g; $d = 0.40$), as shown in Table 7. There was also a decrease in $\text{CEST}_{\text{asym}}$ decay times as shown in Figure 18 (196.0 ± 99.4 vs 247.6 ± 145.1 , $d = 0.44$).

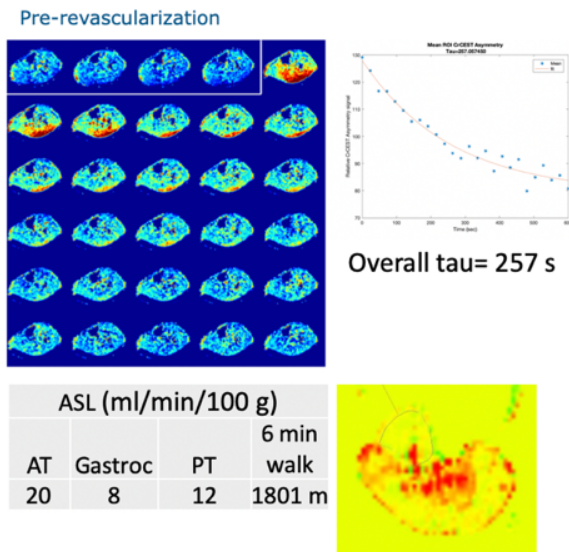


Figure 18: CrCEST and ASL results from a 39-year-old patient with intermittent claudication due to iliac artery compression pre-revascularization (top), 6-weeks post-revascularization (bottom left), and 6-months post-revascularization (bottom right). The tau time-constant of the CrCEST decay initially elongates at 6 weeks post revascularization, when the 6-minute walk score also worsens. At 6 months the decay shortens and the walk score improves.

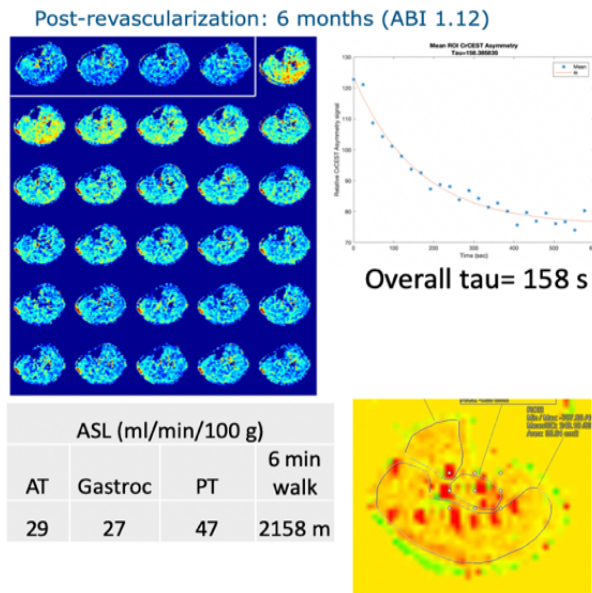
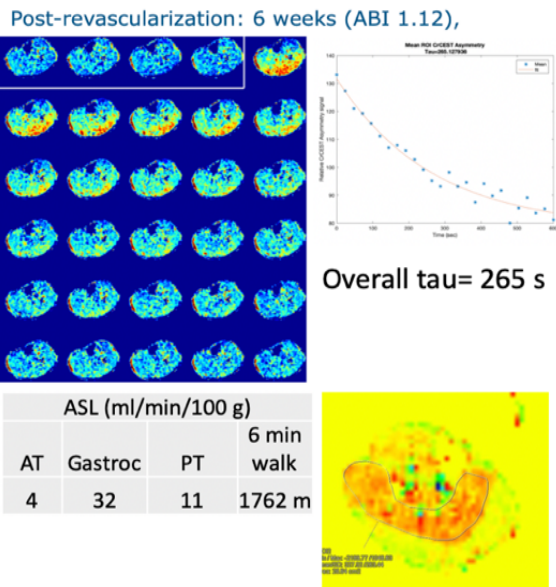


Table 4: ABI, CEST, ASL, and 6-min walk score changes post-revascularization

		Pre-procedure	6-8 weeks Post	6 months Post	p value* pre vs 6-8 weeks	p value* pre vs 6 months
Mean ABI		0.57 (0.22)	0.91 (0.29)	0.91 (0.36)	0.0033	0.0026
Mean CEST decay (s)	Gastrocnemius	397.5 (335.6)	423.7 (192.8)	169.7 (57.5)	0.2829	0.1368
	Anterior Tibialis	198.0 (127.7)	238.7 (154.7)	199.2 (94.2)	0.3808	0.483
	Posterior Tibialis	463.3 (864.8)	268.6 (864.8)	233.8 (168.9)	0.2277	0.2207
	Overall Calf	295.5 (180.5)	345.1 (191.2)	182.0 (81.3)	0.2731	0.1863
Mean ASL flow (mL/min/100g)	Gastrocnemius	7.4 (8.6)	23.9 (7.9)	23.5 (8.6)	0.0003	0.0045
	Anterior Tibialis	15.8 (10.4)	14.3 (10.3)	28.7 (7.1)	0.4021	0.0025
	Posterior Tibialis	10.3 (9.3)	33.3 (12.4)	27.0 (13.9)	0.0016	0.0054
6-min walk score (m)		311.4 (117.1)	414.0 (97.5)	433.9 (126.5)	0.013	0.0045

*p value from 1-tailed paired t -test with 95%

confidence intervals, significant values bolded

Table 5: ABI, CEST, ASL, and 6-minute walk score correlation results post-revascularization

CEST vs ASL	Gastrocnemius		Anterior Tibialis		Posterior Tibialis	
	r	p	r	p	r	p
Pre-procedure	-0.169717672	0.358004941	-0.066699128	0.443509873	-0.61946617	0.068961286
6-8 weeks post	0.31065504	0.248845454	0.213736494	0.322690325	0.364360964	0.21083504
6 months post	-0.394507024	0.219469586	0.680578278	0.068375009	-0.390405383	0.222072005

CEST vs 6 min walk	Gastrocnemius		Anterior Tibialis		Posterior Tibialis		Overall Calf	
	r	p	r	p	r	p	r	p
Pre-procedure	0.312341773	0.247616956	0.036636881	0.468922516	0.080030673	0.432285195	0.295134334	0.260248712
6-8 weeks post	0.376874622	0.202324813	-0.034764689	0.470508645	-0.517369487	0.117176298	-0.033547946	0.471539641
6 months post	-0.32570502	0.264359238	-0.347767261	0.249689477	0.113929702	0.414922425	-0.389090691	0.222908244

ASL vs 6 min walk	Gastrocnemius		Anterior Tibialis		Posterior Tibialis	
	r	p	r	p	r	p
Pre-procedure	0.356601344	0.216180375	0.588452777	0.082288295	0.038354778	0.467467395
6-8 weeks post	0.103728545	0.412425389	-0.740155328	0.02857016	-0.453038565	0.153665739
6 months post	0.494843495	0.159160471	-0.177136527	0.368537124	0.706149423	0.058417757

CEST vs ABI	Overall Calf	
	r	p
Pre-procedure	0.106413686	0.410183812
6-8 weeks post	-0.105398512	0.411031062
6 months post	0.621954442	0.093681412

ABI vs 6 min walk	r	p
	Pre-procedure	0.746879428
6-8 weeks post	0.260117744	0.286598393
6 months post	0.083556373	0.437478561

r values calculated using Pearson correlation

p values from 1-tailed t distribution, significant values bolded

Beet juice subject characteristics	
Variable	All Subjects (n = 5)
Age	72.2 ± 5.2
Weight	91 ± 18
ABI	29.1 ± 4.1
Height	176.4 ± 8.7
ABI	0.67 ± 0.08
Smoker	
Current	4 (80%)
Medications	
ASA/Plavix (blood thinner)	4 (80%)
Alpha-blocker	1 (20%)
Ca ²⁺ channel blockers	1 (20%)
Ace-inhibitors	3 (60%)
Proton pump inhibitor	1 (20%)
Statin	5 (100%)
Phosphodiesterase-3 inhibitor	1 (20%)

Table 6: Beet juice subject characteristics

Data presented as mean ± SD. Medications are presented as number of subjects and percentage (%).

Table 7: ASL flow results for the beetroot juice supplementation group

Perfusion (ml/min-100g)	Placebo (n = 5)	BRJ (n = 5)	Difference BRJ-PL
Anterior compartment	123.9 ± 147.7	97.1 ± 217.1	-26.8 ± 106.1
Lateral compartment	92.1 ± 80.3	121.3 ± 106.5	29.2 ± 127.6
Lateral gastrocnemius	8.2 ± 18.4	27.3 ± 44.4	19 ± 26.5
Medial gastrocnemius	80 ± 29.2	78.5 ± 50.3	-1.5 ± 72.6
Soleus	58.9 ± 45.2	104.8 ± 152.2	45.9 ± 142.7
Deep compartment	26.7 ± 59.8	39.4 ± 71.2	12.7 ± 105.9
Average perfusion	65 ± 32.3	78.1 ± 76.2	
Overall calf perfusion	389.8 ± 193.9	468.3 ± 457.3	78.6 ± 314.9

Data presented as mean ± SD.

A positive value indicates an

Table 8: CEST_{asym} decay results for the beetroot juice supplementation group

	Placebo (n = 5)	BRJ (n = 5)	Difference	P-value
Calf CEST _{asym} decay constant (s), mean±SD	247.6 ± 145.1	196 ± 99.4	-51.5 ± 195.4	0.587
Tibialis anterior CEST _{asym} decay constant (s), mean±SD	181.5 ± 77.9	160.4 ± 102.1	-21.2 ± 143.4	0.758
Tibialis posterior CEST _{asym} decay constant (s), mean±SD	214.9 ± 116.2	210 ± 211.4	-5 ± 249.7	0.967
Gastrocnemius CEST _{asym} decay constant (s), mean±SD	263.5 ± 169.5	200.6 ± 113	-63 ± 231.5	0.576

CEST_{asym} indicates chemical exchanges saturation transfer asymmetry; and BRJ, beetroot juice.

Six subjects were scanned under the non-intervention arm. Their average age was 66±5.4 years and their average lowest ABI was 0.67±13. Their health outcomes were tracked via their electronic medical records for death, cardiovascular, and limb events. The results at an average of 3 years post-enrollment are shown in Figure 19. Four subjects had no relevant health events, and two have since died. One death was from an unrelated cancer, and one was during recovery from an emergent tibioperoneal balloon angioplasty due to CLTI.

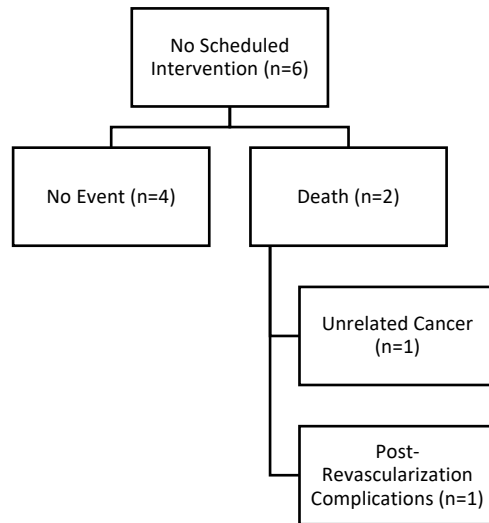


Figure 19: Non-intervention subject health outcomes at an average of 3 years post-enrollment

4.5 Discussion:

This combination of ASL and CrCEST provides a novel methodology to compare metabolism and perfusion on a muscle-group specific basis. The purpose of this study is not to necessarily compare the efficacy of endovascular versus surgical revascularization, as the patient population referred to each group may differ in terms of severity of symptoms. This serves as a study of the utility of CrCEST and ASL in correlating imaging to functional outcomes. Data suggest that revascularization significantly increases perfusion at 6-8 weeks and 6 months but does not significantly improve metabolic function as seen on CrCEST imaging, but low power due to small study size may hinder these findings. Beetroot juice supplementation provides modest improvements in ASL perfusion, walking speed, and CrCEST metabolic function. Further investigation using these imaging techniques would be useful in determining nitrate supplementations efficacy compared to revascularization procedures. The non-intervention group was small, but with 17% of subjects dying from a cardiovascular or revascularization complication agrees

with the national trend of morbidity and mortality in PAD.^[26-29] The combination of ASL and CrCEST imaging is a powerful tool in assessing PAD treatment worthy of further investigation and use.

4.6 Limitations

The significance of this study is hindered by its low power. Patient recruitment was greatly affected by COVID-19, as scheduled procedures were canceled, and human research was paused during most of 2020 at the University of Virginia. Restructuring of the interventional radiology department post-COVID led to fewer endovascular revascularizations being scheduled than expected. We also had difficulty scheduling patients undergoing surgical bypass as many were admitted inpatient and could not travel to our research scanner. Multiple visit studies are difficult to arrange with patients, and several stopped returning after revascularization. The ergometer device was also nonoperational for several months of the study, causing missed timepoints.

4.7 Future Directions

Further patient recruitment is required to prove significance. Recruitment of inpatient subjects may aid in visit compliance and broaden the recruitment pool. Protocol improvements like combining the CEST and ASL into a single post-exercise period would significantly reduce scanner time and improve subject experience.

Chapter 5: Future plans- Creating a combined CrCEST and ASL imaging protocol

The imaging protocol developed in chapter 2 involves two exercise periods to establish sufficient perfusion and metabolic endogenous contrast within the tissue. This extends total scanner time to around 1 hour with exercise and recovery time, with actual imaging time being around 25 min. Some patients are not able to exercise as long during the second protocol due to their claudication pain. In addition, ischemic preconditioning may alter the response to exercise. Removing the need for two exercise periods would greatly increase the clinical feasibility of this protocol. We plan to develop a

single imaging protocol that can measure both CEST and ASL signal within the period of post-exercise hyperemia and increased metabolic energetics seen after plantarflexion. This can be achieved by interleaving ASL imaging in the deadtime of our CEST sequence, as shown in Figure 22. The majority of the CEST imaging sequence is T1 recovery after off-resonant saturation during the CEST prep-pulse. This should allow for ASL tagging and readout in an adjacent slice during that time.^[18] The CEST prep-pulse is not slice selective; however, doing the ASL imaging during a ± 2.3 ppm saturation recovery would limit the amount of on-resonance signal reduction during the ASL readout. The ASL sequence used in Chapter 4 was a PASL sequence with PICORE tagging shown in Figures 19, 20 and 24.

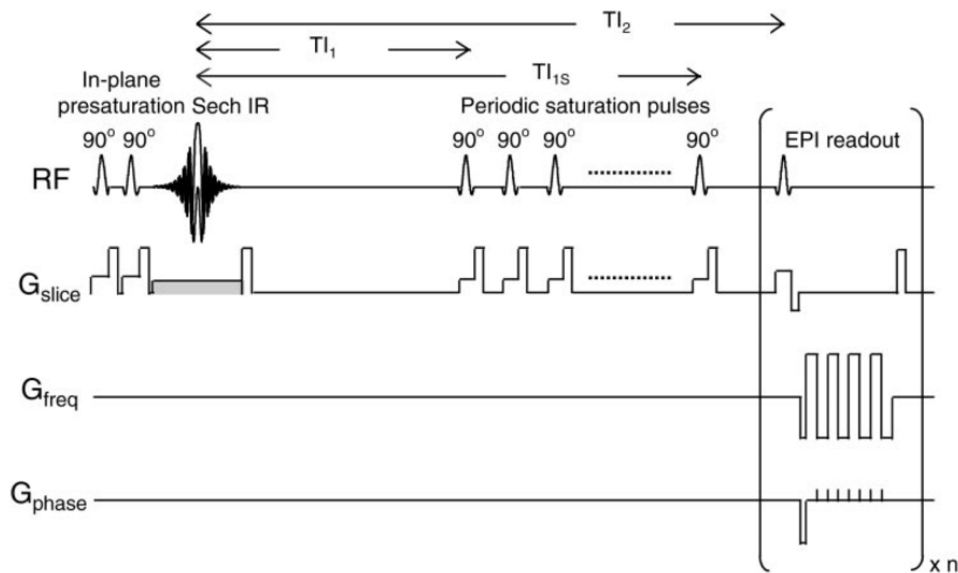


Figure 19: Q2TIPS pulse sequence diagram, where the sech IR is the inversion tagging pulse, and the applied gray gradient alternates negativity between control and tag slices

Adapted from

Luh W-M, Wong EC, Bandettini PA, Hyde JS. QUIPSS II with thin-slice T1 periodic saturation: a method for improving accuracy of quantitative perfusion imaging using pulsed arterial spin labeling. *Magn Reson Med* 1999; 41:1246-1254

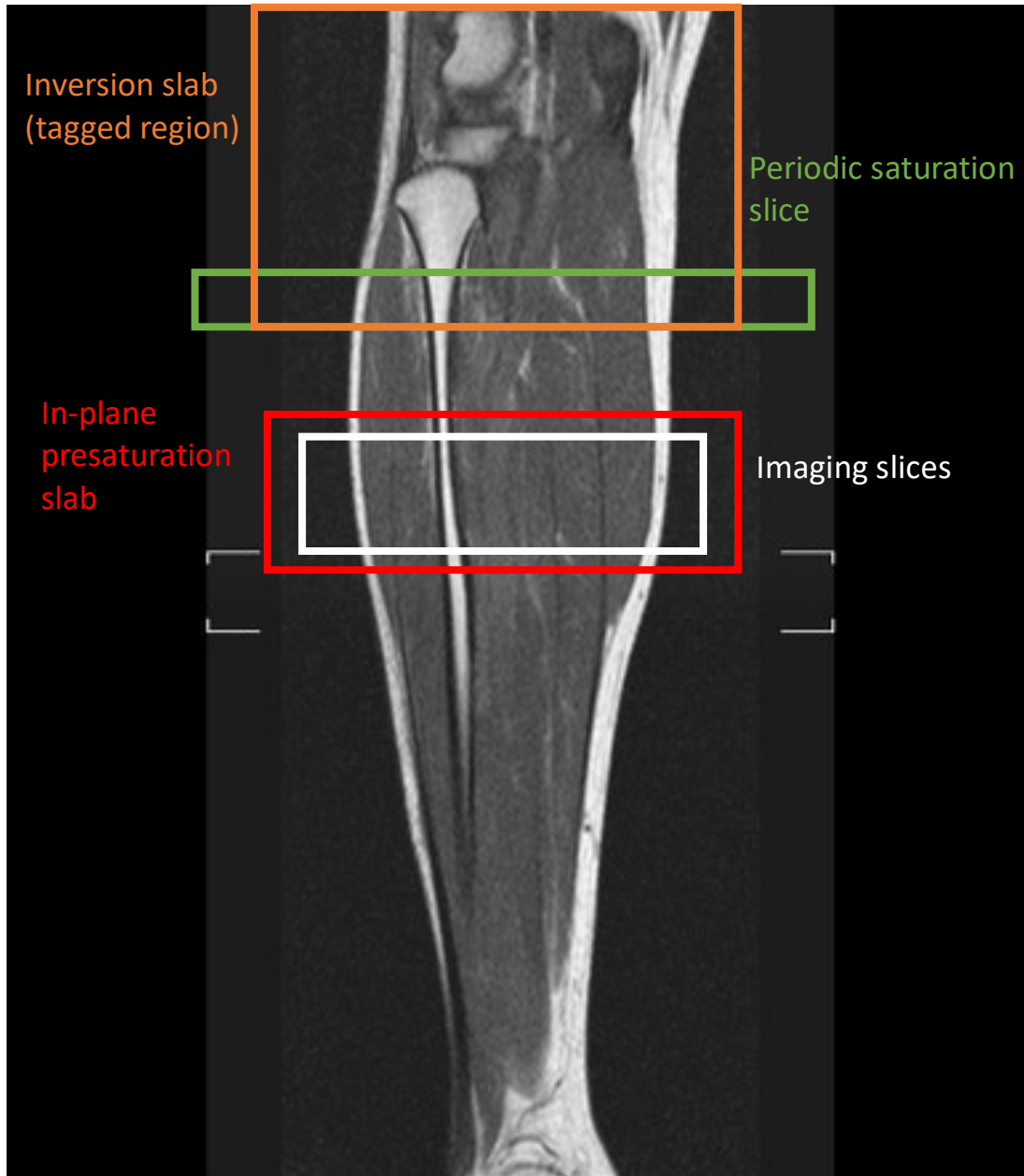
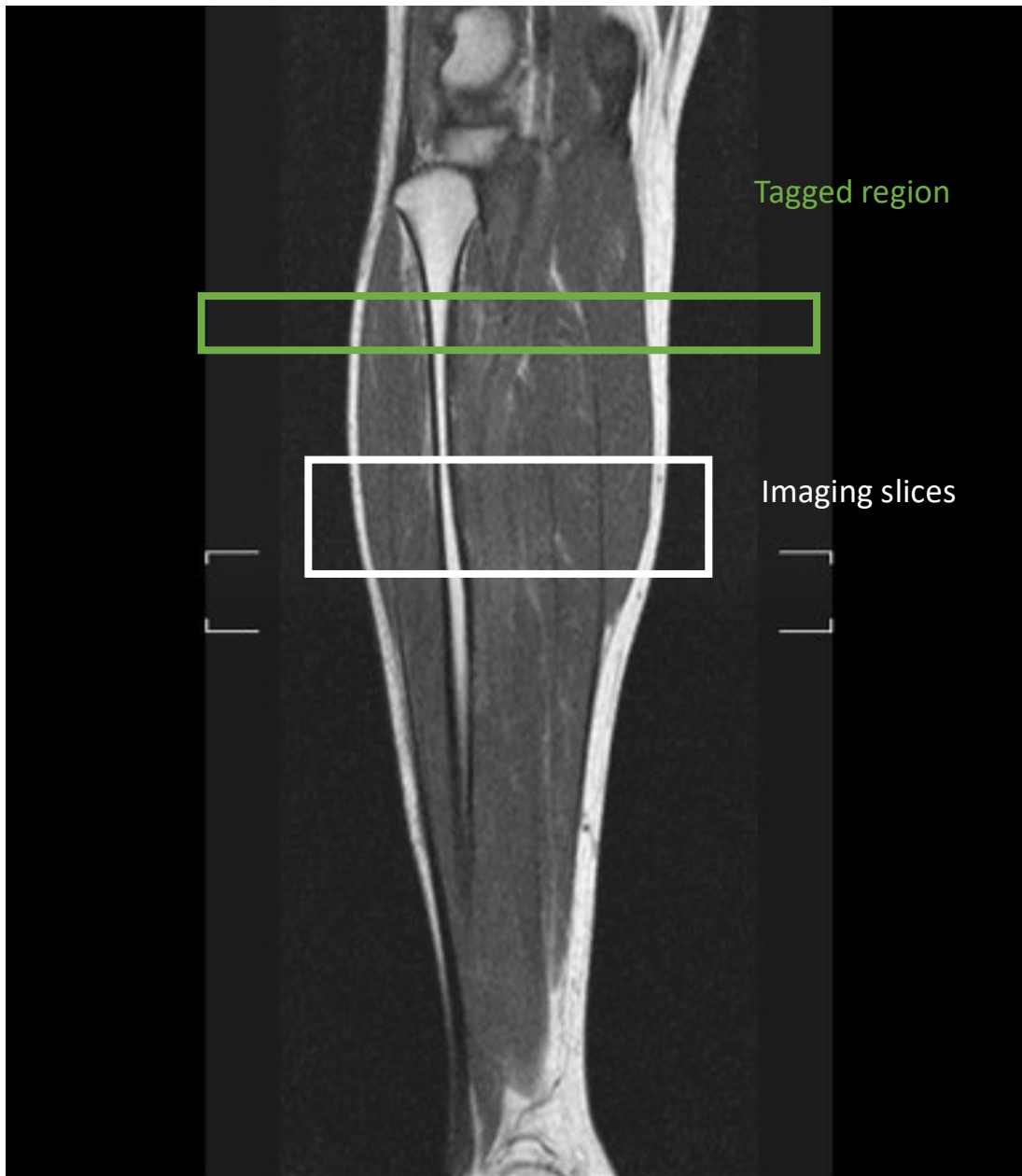
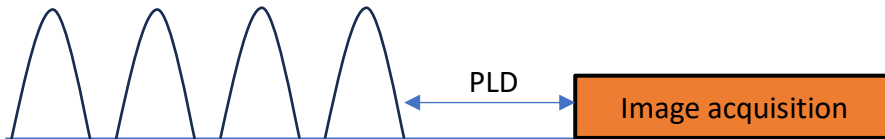


Figure 20: An example of locations of the in-plane presaturation slab, imaging slices, periodic saturation slice, and inversion slab from the PICORE tagging scheme in the leg.

Tatco V, Normal MRI of the leg. Case study, Radiopaedia.org <https://doi.org/10.53347/rID-43617>



RF tagging



RF control

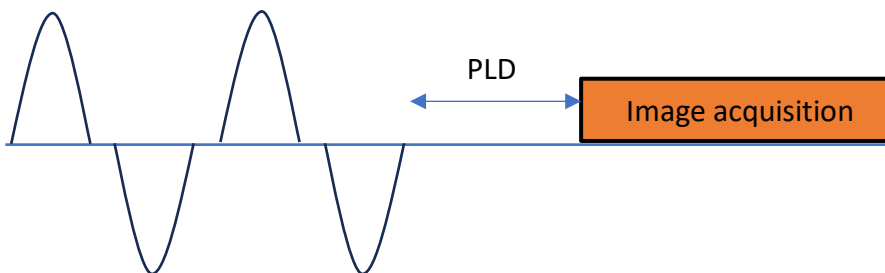


Figure 21: pCASL tagging scheme.

Adapted from Knutsson, L, Xu, J, Ahlgren, A, Zijl, PCM. CEST, ASL, and magnetization transfer contrast: How similar pulse sequences detect different phenomena. *Magn. Reson. Med.* 2018; 80: 1320– 1340. <https://doi.org/10.1002/mrm.27341>

Tatco V, Normal MRI of the leg. Case study, *Radiopaedia.org* <https://doi.org/10.53347/rID-43617>

A pCASL tagging sequence, like shown in Figures 21 and 23, may provide improved SNR and tagging efficiency, but may have too long of an acquisition time to fit within the CEST T1 recovery time. [20,64,65]

Figure 26 shows a simplified overall timing sequence of the combined acquisition.

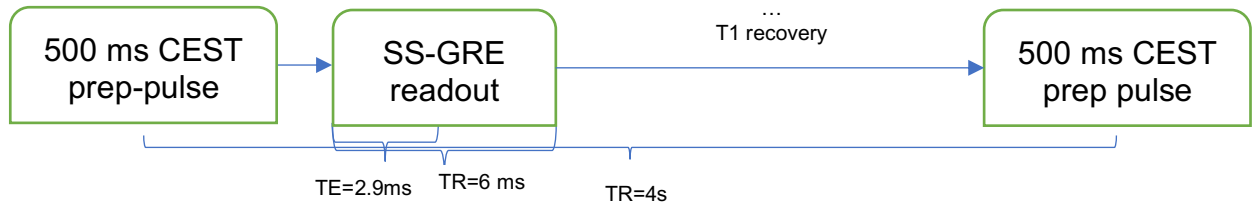


Figure 22: Simplified timing diagram of our CEST pulse sequence

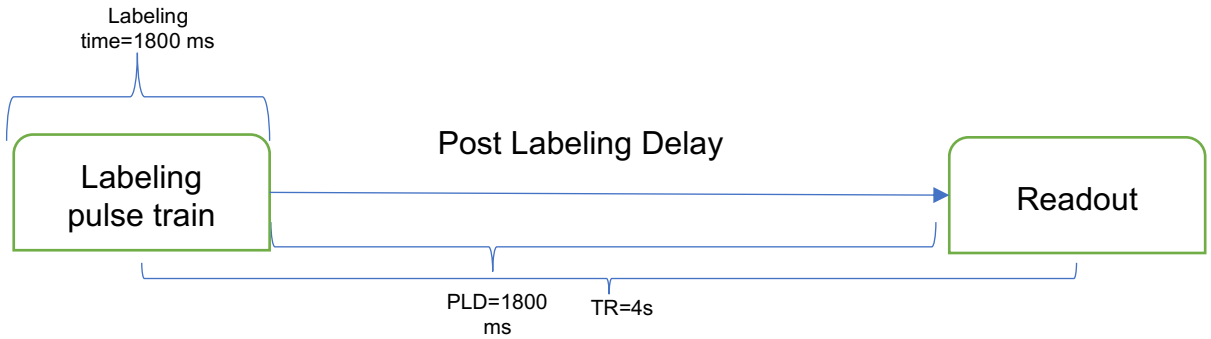


Figure 23: Simplified timing diagram of the pCASL sequence

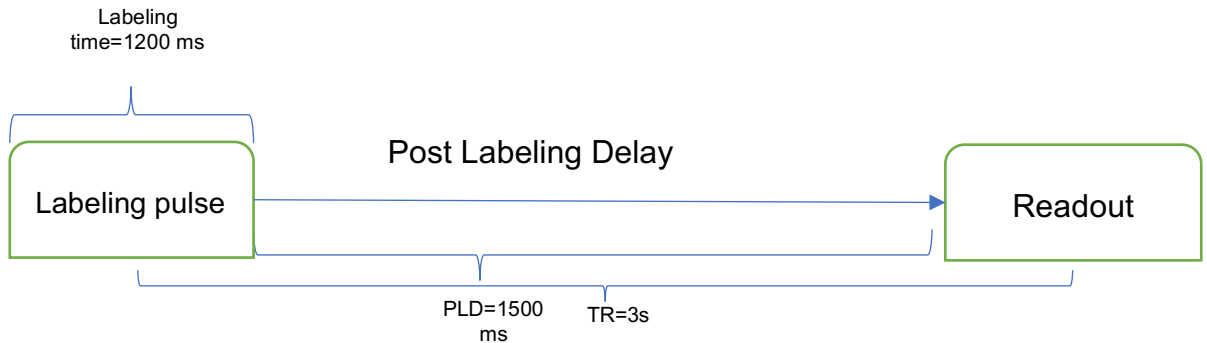


Figure 24: Simplified timing diagram of the PASL sequence

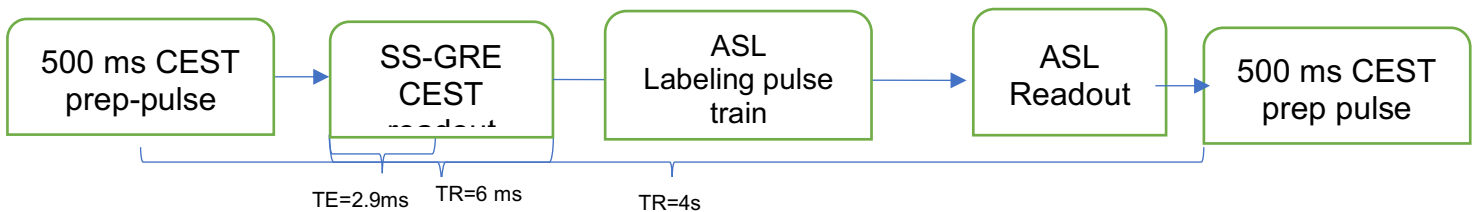


Figure 26: Simplified timing diagram of our CEST and ASL pulse sequence

Expected Outcomes and Alternative Methods:

It is possible that we will not be able to fit a PASL or pCASL acquisition within the 3.5 second T1 recovery gap. A method we explored was running a PASL sequence before starting the CEST acquisition. This causes a delay in beginning the CEST acquisition and missing the beginning of the exponential decay when the signal is highest. We were still able to fit an exponential to the remaining signal, but the signal becomes noisier as the CEST effect decays. There may be intermediate methods available as well, such as placing the ASL acquisition after the first CEST image is acquired, 24 seconds post-exercise. This would occur during the period of increased hyperemia, but still allow sampling of the period of highest creatine concentration. Extending the TR of the CEST sequence is a possibility as well, though this would decrease the number of timepoint samples of the creatine kinetics decay. We plan to assess the quality of measurements from the combined sequence versus our protocol used in Chapter 4 in volunteer studies after development. Healthy volunteers would be more capable than patients of doing three exercise sessions necessary to acquire both sets of imaging. Bland-Altman analysis will be used to show agreement between the two methods.

Chapter 6. Conclusions

Our studies examined the utility of advanced endogenous contrast imaging in PAD. We found that patients with PAD demonstrated a significant increase in creatine decay times in the entire calf compared to their normal age-matched controls. In addition, the difference in creatine decay was also able to be isolated to the specific muscle groups of the calf including the gastrocnemius and posterior tibialis muscles. Measuring tissue energetics in exercising skeletal muscle in PAD has been performed with ^{31}P MRS for over 25 years, which lacks spatial resolution and suffers from low SNR.^[10] ASL and CrCEST are a powerful combination of quantitative MRI measures in assessing PAD and subjects' response to treatment. While ASL perfusion results mirror that of ABI measurements, CEST provides

insight into metabolic functioning and may provide an explanation for lack of functional improvement post-revascularization in some patients. Continued pulse sequence development will aid in the clinical usefulness and viability of a combined CrCEST and ASL protocol by shortening overall scanner time and decreasing painful exercise intervals.

Appendix

The suitability of a solute that exchanges protons with free water for CEST imaging can be expressed as its proton transfer rate (PTR)

$$PTR = x_s \alpha k_{SW} T_{1w} \left(1 - e^{-\frac{t_{sat}}{T_{1w}}} \right) \quad A - 1^{[78,79]}$$

Where α is saturation efficiency, k_{SW} is the exchange rate between the creatine amine proton and water, t_{sat} is the saturation time, and T_{1w} is the T1 of water. x_s is a ratio of solute concentration expressed as

$$x_s = \frac{[\text{creatine amine protons}]}{[\text{water protons}]} \quad A - 2^{[78,79]}$$

The expected CEST signal can be derived from the PTR as follows

$$1 - \frac{S_{sat}(\Delta\omega)}{S_0} = PTR = \frac{[\text{Creatine}]PTE}{2[H_2O]} \quad A - 3^{[78,79]}$$

Where the proton transfer enhancement (PTE) is

$$PTE = N_E \alpha k_{SW} T_{1w} \left(1 - e^{-\frac{t_{sat}}{T_{1w}}} \right) \quad A - 4^{[78-80]}$$

Where N_E is the number of exchangeable protons per kilodalton.

References

1. Selvin E and Erlinger TP. Prevalence of and risk factors for peripheral arterial disease in the United States: Results from the National Health and Nutrition Examination Survey, 1999-2000. *Circulation*. 2004;110:738-743.
2. Virani SS, Alonso A, Aparicio HJ, Benjamin EJ, Bittencourt MS, Callaway CW, Carson AP, Chamberlain AM, Cheng S, Delling FN, Elkind MSV, Evenson KR, Ferguson JF, Gupta DK, Khan SS, Kissela BM, Knutson KL, Lee CD, Lewis TT, Liu J, Loop MS, Lutsey PL, Ma J, Mackey J, Martin SS, Matchar DB, Mussolino ME, Navaneethan SD, Perak AM, Roth GA, Samad Z, Satou GM, Schroeder EB, Shah SH, Shay CM, Stokes A, VanWagner LB, Wang NY and Tsao CW. Heart Disease and Stroke Statistics-2021 Update: A Report From the American Heart Association. *Circulation*. 2021;143:e254-e743.
3. Nehler MR, Duval S, Diao L, Annex BH, Hiatt WR, Rogers K, Zakharyan A and Hirsch AT. Epidemiology of peripheral arterial disease and critical limb ischemia in an insured national population. *J Vasc Surg*. 2014;60:686-695.
4. Greenland P, Abrams J, Aurigemma GP, Bond MG, Clark LT, Criqui MH, Crouse JR, III, Friedman L, Fuster V, Herrington DM, Kuller LH, Ridker PM, Roberts WC, Stanford W, Stone N, Swan HJ, Taubert KA and Wexler L. Prevention Conference V : Beyond Secondary Prevention : Identifying the High-Risk Patient for Primary Prevention : Noninvasive Tests of Atherosclerotic Burden : Writing Group III. *Circulation*. 2000;101:e16-e22.
5. Tehan PE, Barwick AL, Sebastian M and Chuter VH. Diagnostic accuracy of the postexercise ankle-brachial index for detecting peripheral artery disease in suspected claudicants with and without diabetes. *Vasc Med*. 2018;23:116-125.
6. Isbell DC, Berr SS, Toledano AV, Epstein FH, Meyer CH, Rogers WJ, Harthun NL, Hagspiel KD, Weltman A and Kramer CM. Delayed calf muscle phosphocreatine recovery after exercise identifies peripheral arterial disease. *J Am Coll Cardiol*. 2006;47:2289-2297.

7. Haris M, Singh A, Cai K, Kogan F, McGarvey J, Debrosse C, Zsido GA, Witschey WRT, Koomalsingh K, Pilla JJ, Chirinos JA, Ferrari VA, Gorman JH, Hariharan H, Gorman RC and Reddy R. A technique for in vivo mapping of myocardial creatine kinase metabolism. *Nat Med*. 2014;20:209-214.
8. Kogan F, Haris M, Debrosse C, Singh A, Nanga RP, Cai K, Hariharan H and Reddy R. In vivo chemical exchange saturation transfer imaging of creatine (CrCEST) in skeletal muscle at 3T. *JMRI*. 2014;40:596-602.
9. Kogan F, Haris M, Singh A, Cai K, Debrosse C, Nanga RPR, Hariharan H and Reddy R. Method for high-resolution imaging of creatine in vivo using chemical exchange saturation transfer. *Magn Reson Med*. 2014;71:164-172.
10. Schunk K, Romaneehsen B, Mildenerger P, Kersjes W, Schadmand-Fischer S and Thelen M. Dynamic phosphorus-31 magnetic resonance spectroscopy in arterial occlusive disease. Correlation with clinical and angiographic findings and comparison with healthy volunteers. *Invest Radiol*. 1997;32:651-659.
11. Anderson JD, Epstein FH, Meyer CH, Hagspiel KD, Wang H, Berr SS, Harthun NL, Weltman A, Dimaria JM, West AM and Kramer CM. Multifactorial determinants of functional capacity in peripheral arterial disease: uncoupling of calf muscle perfusion and metabolism. *J Am Coll Cardiol*. 2009;54:628-634.
12. Kumar D, Nanga RPR, Thakuri D, Wilson N, Cember A, Martin ML, Zhu D, Shinohara RT, Qin Q, Hariharan H and Reddy R. Recovery kinetics of creatine in mild plantar flexion exercise using 3D creatine CEST imaging at 7 Tesla. *Magn Reson Med*. 2021;85:802-817.
13. Hata J, Nakashima D, Tsuji O, Fujiyoshi K, Yasutake K, Sera Y, Komaki Y, Hikishima K, Nagura T, Matsumoto M, Okano H and Nakamura M. Noninvasive technique to evaluate the muscle fiber characteristics using q-space imaging. *PloS one*. 2019;14:e0214805.

14. Pollak AW, Meyer CH, Epstein FH, Jiji RS, Hunter JR, DiMaria JM, Christopher JM and Kramer CM. Arterial Spin Labeling MR Imaging Reproducibly Measures Peak-Exercise Calf Muscle Perfusion: A Study in Patients With Peripheral Arterial Disease and Healthy Volunteers. *JACC: Cardiovascular Imaging*. 2012;5:1224-1230.
15. D Lopez, AW Pollak, CH Meyer, FH Epstein, AJ Pesch, RS Jiji, JR Kay, JM Dimaria, JM Christopher and CM Kramer. Arterial spin labeling calf perfusion CMR in peripheral arterial disease: Cuff occlusion hyperemia vs. exercise. *J Cardiovasc Magn Reson*. 2015;17:23.
16. Chou TH, Alvelo JL, Janse S, Papademetris X, Sumpio BE, Mena-Hurtado C, Sinusas AJ and Stacy MR. Prognostic Value of Radiotracer-Based Perfusion Imaging in Critical Limb Ischemia Patients Undergoing Lower Extremity Revascularization. *JACC Cardiovasc Imaging*. 2021;14:1614-1624.
17. Kumar D, Armbruster R, Wilson N, Prakash R, Nanga R and Reddy R. Indirect Inference of Acidification in Exercised Skeletal Muscle using Creatine CEST. *Proc Int Soc Magn Reson Med*. 2021;29; abstract.
18. Mancini DM, Coyle E, Coggan A, Beltz J, Ferraro N, Montain S and Wilson JR. Contribution of intrinsic skeletal muscle changes to ³¹P NMR skeletal muscle metabolic abnormalities in patients with chronic heart failure. *Circulation*. 1989;80:1338-46.
19. Grozinger G, Pohmann R, Schick F et al. Perfusion measurements of the calf in patients with peripheral arterial occlusive disease before and after percutaneous transluminal angioplasty using Mr arterial spin labeling. *J Magn Reson Imaging* 2014 October 1;40(4):980-7.
20. Alsop DC, Detre JA, Golay X et al. Recommended implementation of arterial spin-labeled perfusion MRI for clinical applications: A consensus of the ISMRM perfusion study group and the European consortium for ASL in dementia. *Magn Reson Med* 2015 January 1;73(1):102-16.
21. Farber, A. *et al.* Surgery or endovascular therapy for chronic limb-threatening ischemia. *N. Engl. J. Med.* <https://doi.org/10.1056/NEJMoa2207899> (2022).

22. Conte, M. S. *et al.* Global vascular guidelines on the management of chronic limb-threatening ischemia. *J. Vasc. Surg.* **69**, 3S-125S.e40 (2019).
23. Bock JM, Treichler DP, Norton SL, Ueda K, Hughes WE, Casey DP. Inorganic nitrate supplementation enhances functional capacity and lower-limb microvascular reactivity in patients with peripheral artery disease. *Nitric Oxide*. 2018 Nov 1;80:45-51. doi: 10.1016/j.niox.2018.08.007. Epub 2018 Aug 15. PMID: 30118808; PMCID: PMC6239203.
24. Aarti A. Kenjale, Katherine L. Ham, Thomas Stabler, Jennifer L. Robbins, Johanna L. Johnson, Mitch VanBruggen, Grayson Privette, Eunji Yim, William E. Kraus, and Jason D. Allen. Dietary nitrate supplementation enhances exercise performance in peripheral arterial disease. *Journal of Applied Physiology* 2011 110:6, 1582-1591
25. Katakami N. Mechanism of Development of Atherosclerosis and Cardiovascular Disease in Diabetes Mellitus. *J Atheroscler Thromb.* 2018 Jan 1;25(1):27-39. doi: 10.5551/jat.RV17014. Epub 2017 Sep 29. PMID: 28966336; PMCID: PMC5770221.
26. Zemaitis MR, Boll JM, Dreyer MA. Peripheral Arterial Disease. [Updated 2023 May 23]. In: StatPearls [Internet]. Treasure Island (FL): StatPearls Publishing; 2024 Jan-. Available from: <https://www.ncbi.nlm.nih.gov/books/NBK430745/>
27. Beeson SA, Neubauer D, Calvo R, Sise M, Martin M, Kauvar DS, Reid CM. Analysis of 5-year Mortality following Lower Extremity Amputation due to Vascular Disease. *Plast Reconstr Surg Glob Open*. 2023 Jan 11;11(1):e4727. doi: 10.1097/GOX.0000000000004727. PMID: 36699221; PMCID: PMC9833438.
28. Smolderen KG, Samaan Z, Decker C, Collins T, Lazar RM, Itoga NK, Mena-Hurtado C; American Heart Association Council on Peripheral Vascular Disease; Council on Cardiovascular and Stroke Nursing; Council on Clinical Cardiology; Council on Lifestyle and Cardiometabolic Health; and Council on Quality of Care and Outcomes Research. Association Between Mental Health Burden, Clinical

Presentation, and Outcomes in Individuals With Symptomatic Peripheral Artery Disease: A Scientific Statement From the American Heart Association. *Circulation*. 2023 Nov 7;148(19):1511-1528. doi: 10.1161/CIR.0000000000001178. Epub 2023 Oct 2. PMID: 37781785.

29. Kullo IJ, Rooke TW. Peripheral Artery Disease. *New England Journal of Medicine* 2016 March 2;374:861-71.

30. Herrington W et Al. Epidemiology of Atherosclerosis and the Potential to Reduce the Global Burden of Atherothrombotic Disease. *Circulation Research: Compendium on Atherosclerosis* 2016 February 19; 535-46.

31. Johnston AL, Vemulapalli S, Gosch KL, Aronow HD, Abbott JD, Patel MR, Smolderen KG, Shishebor M, Spertus JA, Jones WS. Ankle-brachial index in patients with intermittent claudication is a poor indicator of patient-centered and clinician-based evaluations of functional status. *J Vasc Surg*. 2019 Mar;69(3):906-912. doi: 10.1016/j.jvs.2018.07.039. Epub 2019 Jan 6. PubMed PMID: 30626552.

32. Høyer C, Sandermann J, Petersen LJ. The toe-brachial index in the diagnosis of peripheral arterial disease. *J Vasc Surg*. 2013 Jul;58(1):231-8. doi: 10.1016/j.jvs.2013.03.044. Epub 2013 May 18. PMID: 23688630.

33. Barclay CJ. Energetics of contraction. *Compr Physiol*. 2015 Apr;5(2):961-95. doi: 10.1002/cphy.c140038. PMID: 25880520.

34. Clark JF. Creatine and phosphocreatine: a review of their use in exercise and sport. *J Athl Train*. 1997 Jan;32(1):45-51. PMID: 16558432; PMCID: PMC1319235.

35. Sunner SS, Welsh RC, Baine KR. Medical Management of Peripheral Arterial Disease: Deciphering the Intricacies of Therapeutic Options. *CJC Open*. 2021 Mar 12;3(7):936-949. doi: 10.1016/j.cjco.2021.03.005. PMID: 34401701; PMCID: PMC8348339.

36. Treat-Jacobson D, McDermott MM, Bronas UG, Campia U, Collins TC, Criqui MH, Gardner AW, Hiatt WR, Regensteiner JG, Rich K; American Heart Association Council on Peripheral

Vascular Disease; Council on Quality of Care and Outcomes Research; and Council on Cardiovascular and Stroke Nursing. Optimal Exercise Programs for Patients With Peripheral Artery Disease: A Scientific Statement From the American Heart Association. *Circulation*. 2019 Jan 22;139(4):e10-e33. doi: 10.1161/CIR.0000000000000623. PMID: 30586765.

37. Kazi DS, Penko J, Coxson PG, Moran AE, Ollendorf DA, Tice JA, Bibbins-Domingo K. Updated Cost-effectiveness Analysis of PCSK9 Inhibitors Based on the Results of the FOURIER Trial. *JAMA*. 2017 Aug 22;318(8):748-750. doi: 10.1001/jama.2017.9924. PMID: 28829863; PMCID: PMC5817484.

38. Beckman, Joshua A. et al. "Advances in Revascularization for Peripheral Artery Disease." *Circulation Research* 128 (2021): 1885 - 1912.

39. Arabzadeh A, Faghfuri E, Razi Soofiyan S, Dalir Abdolahinia E, Siapush S, Nejati-Koshki K, Shahrami B, Asghariazar V, Pahlavan Y. Current and Novel Emerging Medical Therapies for Peripheral Artery Disease: A Literature Review. *Adv Pharm Bull*. 2023 Mar;13(2):259-268. doi: 10.34172/apb.2023.025. Epub 2022 Apr 4. PMID: 37342373; PMCID: PMC10278215.

40. Madabhushi V, Davenport D, Jones S, Khoudoud SA, Orr N, Minion D, Endean E, Tyagi S. Revascularization of intermittent claudicants leads to more chronic limb-threatening ischemia and higher amputation rates. *J Vasc Surg*. 2021 Sep;74(3):771-779. doi: 10.1016/j.jvs.2021.02.045. Epub 2021 Mar 26. PMID: 33775749.

41. Rumenapf G, Morbach S, Schmidt A, Sigl M. Intermittent Claudication and Asymptomatic Peripheral Arterial Disease. *Dtsch Arztebl Int*. 2020 Mar 13;117(11):188-193. doi: 10.3238/arztebl.2020.0188. PMID: 32327031; PMCID: PMC7191120.

42. Baird MF, Graham SM, Baker JS, Bickerstaff GF. Creatine-kinase- and exercise-related muscle damage implications for muscle performance and recovery. *J Nutr Metab*. 2012;2012:960363. doi: 10.1155/2012/960363. Epub 2012 Jan 11. PMID: 22288008; PMCID: PMC3263635.

43. Woessner M, VanBruggen MD, Pieper CF, Sloane R, Kraus WE, Gow AJ, Allen JD. Beet the Best? *Circ Res.* 2018 Aug 31;123(6):654-659. doi: 10.1161/CIRCRESAHA.118.313131. PMID: 29976553; PMCID: PMC6202165.
44. Kim M, Gillen J, Landman BA, Zhou J, van Zijl PC. Water saturation shift referencing (WASSR) for chemical exchange saturation transfer (CEST) experiments. *Magn Reson Med.* 2009 Jun;61(6):1441-50. doi: 10.1002/mrm.21873. PMID: 19358232; PMCID: PMC2860191.
45. Kukovetz WR, Holzmann S, Romanin C. Mechanism of vasodilation by nitrates: role of cyclic GMP. *Cardiology.* 1987;74 Suppl 1:12-9. doi: 10.1159/000174258. PMID: 2886220.
46. Kruse NT, Ueda K, Hughes WE, Casey DP. Eight weeks of nitrate supplementation improves blood flow and reduces the exaggerated pressor response during forearm exercise in peripheral artery disease. *Am J Physiol Heart Circ Physiol.* 2018 Jul 1;315(1):H101-H108. doi: 10.1152/ajpheart.00015.2018. Epub 2018 Mar 9. PMID: 29522355; PMCID: PMC6087779.
47. Meyerspeer M, Krssák M, Moser E. Relaxation times of 31P-metabolites in human calf muscle at 3 T. *Magn Reson Med.* 2003 Apr;49(4):620-5. doi: 10.1002/mrm.10426. PMID: 12652531.
48. Schocke M, Esterhammer R, Greiner A. High-energy phosphate metabolism in the exercising muscle of patients with peripheral arterial disease. *Vasa.* 2008 Aug;37(3):199-210. doi: 10.1024/0301-1526.37.3.199. PMID: 18690587.
49. Šedivý P, Kipfelsberger MC, Dezortová M, Krššák M, Drobný M, Chmelík M, Rydlo J, Trattng S, Hájek M, Valkovič L. Dynamic 31P MR spectroscopy of plantar flexion: influence of ergometer design, magnetic field strength (3 and 7 T), and RF-coil design. *Med Phys.* 2015 Apr;42(4):1678-89. doi: 10.1118/1.4914448. PMID: 25832057.
50. I. I. Rabi, N. F. Ramsey and J. Schwinger. Rotating coordinates in magnetic resonance problems. *Rev. Modern Phys.*, 26: 167, 1954.

51. Brown, R.W. et al. (2014) *Magnetic Resonance Imaging: Physical principles and sequence design*. Hoboken, NJ: Wiley Blackwell.
52. Nishimura, Dwight G. *Principles of Magnetic Resonance Imaging / Dwight G. Nishimura*. Ed. 1.1. S.l: D. Nishimura, 2010. Print.
53. Bloch F. Nuclear induction. *Phys Rev* 1946; 70:460-474,1946.
54. Bernstein, M.A.; King, K.F.; Zhou, X.J. (2004). *Handbook of MRI Pulse Sequences*. San Diego, CA: Elsevier Academic Press. p. 960. ISBN 0-12-092861-2
55. Jerrold T. Bushberg, John M. Boone. *The Essential Physics of Medical Imaging*. (2012) ISBN: 9780781780575
56. Rabi II, Zacharias JR, Millman S, Kusch P. Milestones in magnetic resonance: 'a new method of measuring nuclear magnetic moment' . 1938. *J Magn Reson Imaging*. 1992 Mar-Apr;2(2):131-3. doi: 10.1002/jmri.1880020203. PMID: 1562763.
57. Barisano G, Sepehrband F, Ma S, Jann K, Cabeen R, Wang DJ, Toga AW, Law M. Clinical 7 T MRI: Are we there yet? A review about magnetic resonance imaging at ultra-high field. *Br J Radiol*. 2019 Feb;92(1094):20180492. doi: 10.1259/bjr.20180492. Epub 2018 Nov 1. PMID: 30359093; PMCID: PMC6404849.
58. Cooper GM. *The Cell: A Molecular Approach*. 2nd edition. Sunderland (MA): Sinauer Associates; 2000. *The Molecular Composition of Cells*.
59. Heaney RP. Phosphorus. In: Erdman JW, Macdonald IA, Zeisel SH, eds. *Present Knowledge in Nutrition*. 10th ed. Washington, DC: Wiley-Blackwell; 2012:447-58.
60. Tannus A, Garwood M. Adiabatic pulses. *NMR in Biomed* 1997;10:423-434
61. Ho KY, Leiner T, van Engelshoven JM. MR angiography of run-off vessels. *Eur Radiol*. 1999;9(7):1285-9. doi: 10.1007/s003300050835. PMID: 10460361.

62. Wong EC, Buxton RB, Frank LR. Implementation of quantitative perfusion imaging techniques for functional brain mapping using pulsed arterial spin labeling. *NMR in Biomed* 1997; 10:237-249.
63. Luh W-M, Wong EC, Bandettini PA, Hyde JS. QUIPSS II with thin-slice T11 periodic saturation: a method for improving accuracy of quantitative perfusion imaging using pulsed arterial spin labeling. *Magn Reson Med* 1999; 41:1246-1254
64. Dai W, Garcia D, de Bazelaire C, Alsop DC. Continuous flow driven inversion for arterial spin labeling using pulsed radiofrequency and gradient fields. *Magn Reson Med* 2008; 60:1488-1497.
65. Knutsson, L, Xu, J, Ahlgren, A, Zijl, PCM. CEST, ASL, and magnetization transfer contrast: How similar pulse sequences detect different phenomena. *Magn. Reson. Med.* 2018; 80: 1320– 1340. <https://doi.org/10.1002/mrm.27341>
66. Pollak AW, Kramer CM. MRI in Lower Extremity Peripheral Arterial Disease: Recent Advancements. *Curr Cardiovasc Imaging Rep.* 2013 Feb 1;6(1):55-60. doi: 10.1007/s12410-012-9175-z. PMID: 23336015; PMCID: PMC3547388.
67. R I Grossman, J M Gomori, K N Ramer, F J Lexa, and M D Schnall. Magnetization transfer: theory and clinical applications in neuroradiology. *RadioGraphics* 1994 14:2, 279-290
68. Balaban RS, Ceckler TL. Magnetization Transfer Contrast in Magnetic Resonance Imaging. *Magn Reson Q* 1992; 8(2): 116-137
69. Rydzy M, Deslauriers R, Smith IC, Saunders JK. Optimization of magnetization transfer measurements: statistical analysis by stochastic simulation. Application to creatine kinase kinetics. *Magn Reson Med.* 1990 Aug;15(2):260-74. doi: 10.1002/mrm.1910150209. PMID: 2392051.
70. Forsén S, Hoffman RA. Study of Moderately Rapid Chemical Exchange Reactions by Means of Nuclear Magnetic Double Resonance. *J Chem Phys* 1963; 39: 2892-2901

71. Halle B. Water in biological systems: the NMR picture. In: Bellissent-Funel M-C (ed.). Hydration processes in biology : theoretical and experimental approaches. IOS Press, Clifton, VA. 1999: 233-249.
72. Overhauser AW. Polarization of nuclei in metals. *Phys Rev* 1953; 92:411-415.
73. van Faassen EE, Bahrami S, Feelisch M, Hogg N, Kelm M, Kim-Shapiro DB, Kozlov AV, Li H, Lundberg JO, Mason R, Nohl H, Rassaf T, Samouilov A, Slama-Schwok A, Shiva S, Vanin AF, Weitzberg E, Zweier J, Gladwin MT. Nitrite as regulator of hypoxic signaling in mammalian physiology. *Med Res Rev*. 2009 Sep;29(5):683-741. doi: 10.1002/med.20151. PMID: 19219851; PMCID: PMC2725214.
74. Mason, S., Johnson, R.S. (2007). The Role of Hif-1 1 in Hypoxic Response in the Skeletal Muscle. In: Roach, R.C., Wagner, P.D., Hackett, P.H. (eds) Hypoxia and the Circulation. *Advances in Experimental Medicine and Biology*, vol 618. Springer, Boston, MA. https://doi.org/10.1007/978-0-387-75434-5_18
75. Favier, F.B., Britto, F.A., Freyssenet, D.G. *et al.* HIF-1-driven skeletal muscle adaptations to chronic hypoxia: molecular insights into muscle physiology. *Cell. Mol. Life Sci.* **72**, 4681–4696 (2015). <https://doi.org/10.1007/s00018-015-2025-9>
76. Nair KS, Irving BA, Lanza IR. Can dietary nitrates enhance the efficiency of mitochondria? *Cell Metab*. 2011 Feb 2;13(2):117-8. doi: 10.1016/j.cmet.2011.01.013. PMID: 21284976; PMCID: PMC3049330.
77. Ju L, Wang K, Schär M, Xu S, Rogers J, Zhu D, Qin Q, Weiss RG, Xu J. Simultaneous creatine and phosphocreatine mapping of skeletal muscle by CEST MRI at 3T. *Magn Reson Med*. 2024 Mar;91(3):942-954. doi: 10.1002/mrm.29907. Epub 2023 Oct 29. PMID: 37899691; PMCID: PMC10842434.
78. Van Zijl, P. C. M., & Sehgal, A. A. (2016). Proton chemical exchange saturation transfer (CEST) MRS and MRI. *eMagRes*, 5(2), 1307-1332. <https://doi.org/10.1002/9780470034590.emrstm1482>

79. Van Zijl PC, Yadav NN. Chemical exchange saturation transfer (CEST): what is in a name and what isn't? *Magn Reson Med*. 2011 Apr;65(4):927-48. doi: 10.1002/mrm.22761. Epub 2011 Feb 17. PMID: 21337419; PMCID: PMC3148076.

80. Xu J, Chung JJ, Jin T. Chemical exchange saturation transfer imaging of creatine, phosphocreatine, and protein arginine residue in tissues. *NMR Biomed*. 2023 Jun;36(6):e4671. doi: 10.1002/nbm.4671. Epub 2022 Jan 3. PMID: 34978371; PMCID: PMC9250548.